Univerzita Karlova v Praze
Matematicko-fyzikální fakulta

DIPLOMOVÁ PRÁCE

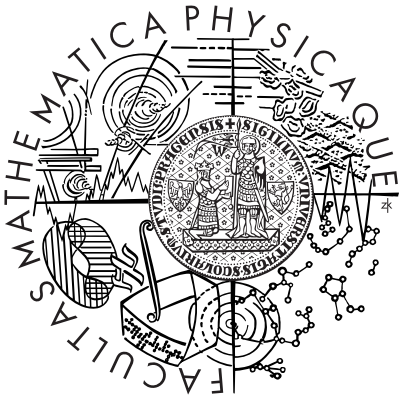

Robert Vácha

Molekulové simulace interakcí molekul a iontů na rozhraní voda/vzduch.

Ústav organické chemie a biochemie
Akademie věd České republiky

Vedoucí diplomové práce: **doc. Pavel Jungwirth, CSc.**

Studijní program: **Fyzika**

Studijní plán: **Biofyzika a chemická fyzika**

Tímto bych rád poděkoval svému školiteli doc. Pavlu Jungwirthovi, CSc. za vedení diplomové práce, množství užitečných nápadů, rad a připomínek. Také bych rád poděkoval všem kolegům z Centra pro komplexní molekulové systemy a biomolekuly za podporu a cenné konzultace. V neposlední řadě bych chtěl poděkovat svým rodičům, bratrovi a partnerce za podporu a trpělivost během celého studia a při psaní této práce.

Prohlašuji, že jsem svou diplomovou práci napsal samostatně a výhradně s použitím citovaných pramenů.
Souhlasím se zapůjčováním práce.

V Praze dne 10.4.2005 Robert Vácha

Contents

Název práce: Molekulové simulace interakcí molekul a iontů na rozhraní voda/vzduch.
Autor: Robert Vácha
Katedra: Katedra chemické fyziky a optiky
Vedoucí diplomové práce: doc. Pavel Jungwirth, CSc.
e-mail vedoucího: Pavel.Jungwirth@uochb.cas.cz
Abstrakt: Pomocí molekulových simulací jsme studovali chování molekul na rozhraní voda/vzduch. K tomuto účelu jsme vyzkoušeli různé techniky získávání profilů koncentrace a volné energie pro přechod rozpouštěné látky ze vzduchu do vody přes rozhraní voda/vzduch. Tento profil volné energie se také nazývá potenciál střední síly (PMF). Po porovnaní výhod a nevýhod jednotlivých metod se ukázalo, že nejvhodnější je nová nepřímá metoda omezujícího harmonického potenciálu v souřadnici kolmé k rozhraní voda/vzduch. Ke studiu jsme vybrali sadu atmosféricky důležitých molekul, radikálů a iontů: N_2, O_2, H_2O, O_3, OH, HO_2, H_2O_2, OH^-, Na^+, F^-, H_3O^+ a $H_5O_2^+$. Simulace neutrálních molekul dobře reprodukují hydratační volnou energii odvozenou z experimentálně zjištěných Henryho konstant. Pro ionty, kde je situace komplikovanější, jsme byli schopni získat alespoň vodní a povrchovou část profilu. Zjistili jsme obecnou závislost změn PMF na různých simulačních parametrech. Z našich simulací plyne, že zvýšená koncentrace na rozhraní voda/vzduch je obecný jev pro všechny neutrální molekuly (jak hydrofobní tak hydrofilní) kromě vody samotné. Zvýšená povrchová koncentrace atmosféricky důležitých molekul má závažné důsledky pro heterogenní chemické procesy probíhajících na vodních částicích v atmosféře.
Klíčová slova: molekulová dynamika, rozhraní voda/vzduch, volná energie, solvatace, hydratace, ionty, atmosférické plyny

Title: Molecular simulations of molecular and ion interactions at the air/water interface.
Author: Robert Vacha
Department: department of chemical physics and optics
Supervisor: doc. Pavel Jungwirth, CSc.
Supervisor's e-mail address: Pavel.Jungwirth@uochb.cas.cz
Abstract: By means of molecular dynamics simulations we studied the behaviour of molecules at the air/water interface. For this purpose we investigated different simulation methods for obtaining the concentration and free energy profiles of the solute moving from the gas phase into the aqueous phase across the air/water interface, i.e. the Potential of Mean Force (PMF). After comparing the advantages and disadvantages of individual methods we chose a novel indirect method employing a constraining harmonic potential in the coordinate perpendicular to the air/water interface. A set of atmospherically relevant molecules, radicals, and ions was selected for our study: N_2, O_2, H_2O, O_3, OH, HO_2, H_2O_2, OH^-, Na^+, F^-, H_3O^+, and $H_5O_2^+$. The hydration free energies of neutral molecules derived from the experimental Henry's law constants were well reproduced. For the ions, where the situation is more complicated, we obtained at least a part of the PMF at the interface and in the bulk water. We found general dependencies of the PMF changes on different simulation parameters. According to our simulations the concentration enhancement at the air/water interface is a generic effect for all neutral species (both hydrophobic and hydrophilic) with the exception of water vapor itself. The surface enhancement of atmospherically relevant gases has important consequences for heterogeneous chemical processes occurring on aqueous particles in the atmosphere.
Keywords: molecular dynamics, air/water interface, free energy, hydration, solvation, ions, atmospheric gases

Chapter 1

Introduction

The Earth's atmosphere is created mostly by gases, however, it also contains liquid and solid particles that significantly influence the atmospheric chemistry. Chemical reactions at the surfaces of these particles are heterogeneous processes, the importance of which has been demonstrated in both the stratosphere and the troposphere over last decades [1]. For example the global atmospheric models from the 1980s did not contain heterogeneous processes, as a result they were not able to predict the creation and development of ozone holes in polar regions. It is known today that activation of chlorine that destroys ozone at the surface of particles forming polar stratospheric clouds is responsible for the Arctic and Antarctic ozone holes [1].

There is a wide range of particles in the atmosphere on which heterogeneous reactions may occur. The main ones are fog and cloud water droplets (present mainly in the lower troposphere) and ice crystals (primarily in the upper troposphere). On average more than half of the Earth is covered by clouds and about seven percent of the volume of the troposphere is filled with clouds. If all the cloud droplets are approximated with spheres of diameter of ten micrometers, there is about one million of them in a litre of air and the total area of water surface is three square centimeters per litre [2]. Thus the water surface area in the troposphere, on which the heterogeneous reactions may occur, is enormous and the effect of the surface reactions on atmospheric processes can be large and global.

The amount of reactants at the surface is important for heterogeneous reactions, because the speed of chemical reactions depends on their concentrations. However, the surface concentrations for a wide variety of substances are not well known. It is difficult to measure these directly, moreover, it is not obvious that the concentration switches monotonously from the gas phase into the aqueous bulk. Chemical processes at the surface usually run much faster than in the bulk, because the reactants do not diffuse in 3D but rather in 2D. Some reactions may even occur pri-

marily at the surface. This concerns cases where the reactants are separated in different phases. For instance the measured release of molecular chlorine from aqueous sea salt aerosols did not agree with the prediction from atmospheric models until the surface reactions of Cl^- with OH were included. The unexpected enhancement of the chloride anion at the surface was confirmed by molecular simulations [3, 4].

Molecular simulation is a type of a computer experiment in which the behaviour of system is based on an interaction model with atomic resolution. It has become a powerful tool to solve many-body problems in physics, physical chemistry, and biochemistry. These molecular experiments provide a solution to statistical mechanical problems, which otherwise would need severe theoretical approximations or which are described only by macroscopic measurable quantities without microscopic details. Molecular simulations bridge both theories and real experiments, and they help us to uncover and understand the underlying molecular processes.

Molecular simulations can be divided into stochastic and deterministic simulations. The stochastic group is covered by Monte Carlo methods, in which the configurations of system are probed randomly or with a Boltzmann type bias. The second group encompasses Molecular Dynamics (MD) approaches that are deterministic time evolution methods based on a numerical solution of Newton's classical equations of motion for all atoms in the system. Interactions between the atoms are described by a force-field that is usually build on a combination of empirical data and *ab initio* quantum chemical calculations. *Ab initio* methods involve only the electronic Schrödinger equation, the fundamental physical constants and atoms configuration of studied system. These quantum methods are highly accurate, but they are computationally expensive and can be used only for small systems (up to tens of atoms). Classical molecular simulations are used for much larger systems (up to thousands of atoms), however, they do not include quantum effects. We employed these simulations to study the behaviour of molecules at the air/water interface.

Recently new surface-specific experimental techniques appeared such as the sum frequency generation (SFG) [5, 6] and the second harmonic generation (SHG) [7, 8]. These are nonlinear spectroscopic methods, where the bulk contributions vanish within the dipole approximation and only few top molecular layers are probed. These methods are capable to characterize hydrogen bonds and ion adsorption at the aqueous surface. For example, the recent results support the theoretically predicted (by MD simulations) surface enhancement of highly polarizable inorganic anions [10].

While the microscopic structure and concentration at the liquid surfaces are difficult to obtain directly from experiments, they are commonly derived from easily measurable macroscopic properties, such as the sur-

face tension. The surface tension of water can be increased or decreased in dependence on the solute. Most of the dissolved substances lower the surface tension compared to pure water. For example it has been known for decades that the water surface tension decreases slightly with increasing atmospheric pressure, which can be interpreted as adsorption of nitrogen and (or) oxygen at the water surface [9].

While the direct measurement of the molecular structure and concentration at the air/water interface is still difficult, it is relatively easy to obtain not only the structure and concentration but also dynamical and macroscopic properties of the surface from molecular simulations. The simulations of the water surface require extended systems, so they are still prohibitively expensive for *ab initio* methods nowadays, but it is computationally feasible to simulate the system by MD. Moreover, due to the continuous advance in computer technology and higher computer performance it is becoming possible to study more complicated systems with higher accuracy.

The aim of this thesis is to study the behaviour of molecules at the air/water interface by means of MD simulations. For this purpose we investigate different simulation methods for obtaining the concentration and free energy profiles of the solute moving from the gas phase into the aqueous phase across the air/water interface. Both direct and indirect computational methods exhibit technical difficulties and, therefore, they are constantly developed and improved. We participate on the development and implementation of several approaches and discuss the advantages and disadvantages of the tested methods. The most suitable technique is chosen and used for further simulations. In particular, we primarily employ indirect methods which yield a Potential of Mean Force (PMF) as a result. This free energy profile can also be easily converted into a concentration profile. A set of atmospherically relevant molecules was chosen for our study: nitrogen (as the most abundant gas), oxygen (as the gas essential for oxidation processes), water vapour (as the gaseous form of the most important solvent), ozone and hydroxyl radical (as the main oxidants during the daytime), peroxide and hydroperoxy radical (as very reactive atmospheric species). In addition, we investigated several atmospherically important ions such as OH^-, Na^+, F^-, H_3O^+, and $H_5O_2{}^+$. Using the simulations we address the following questions. Is the concentration of solute changing monotonously from the gas phase into the aqueous bulk or is there any solute propensity for the air/water interface? Is the enhanced concentration at aqueous surface a generic effect and what are the possible effects this surface increased concentrations? Does the behaviour of hydrophilic and hydrophobic molecules differ from each other and are we able to make quantitative conclusions concerning the investigated ions?

Chapter 2

Simulations

Molecular dynamics (MD) simulations represent a computational chemistry method that stands between experiment and theory and can bridge the two. The experiments can be compared with the microscopic model and theoretical hypothesis can be checked directly. The simulations can even mimic an experiment that cannot be easily performed (e.g., very high temperatures and pressures or very short timescale) and we can also get information of processes on the molecular level.

Classical molecular dynamics is a method based on the solution of the Newton's equations of motion

$$F_i = m_i \frac{\partial^2 r_i}{\partial t^2}, \tag{2.1}$$

where the index i runs over all atoms in the system. The equations are solved simultaneously in small time steps and the force is calculated as a negative derivative of the potential (more details on the potential in Appendix A).

Atoms in a computer are moving, colliding or diffuse in a similar way as the real atoms would do. The computer calculates a time trajectory of the whole system as a set of subsequent configurations in the phase space and it provides sampling of a statistical ensemble. Physically measurable quantities are then obtained as averages over the trajectory. By sufficient MD sampling we are able to get information of both microscopic and macroscopic behaviour and properties. However, thermodynamic properties would be exactly obtained only by an infinite long simulation, where the entire phase space is fully sampled. Real MD simulations are, however, finite, so one should be wary of the sampling quality of simulated system and its parameters. MD is a classical description, so it cannot account for quantum effects. Consequently, one should be aware of these limitations and verify the data against experiments.

2.1 Computational details

For molecular dynamics simulations we used a program package Gromacs [11] version 3.1.5 compiled first in single precision. A double precision version was then used for the final production runs.

Our system consisted of a solute molecule (an atmospheric molecule, radical, or ion), 215 molecules of water, and a very heavy fictitious (XX) particle. The purpose of employing this particle was to create a stationary point for PMF calculations (see below). Water in a rectangular cell with dimensions 1.86nm, 1.86nm, and 38.86nm and x,y,z-periodic boundary conditions yielded an infinite slab (2nm thick in z-direction), as shown in Fig 2.1 and 2.2. The two water/vapor interfaces can be also considered as air/water interfaces since the density of nitrogen (the main part of the atmosphere) is $\sim 10^{25}$ molecules/m^3, so there would be only few molecules of nitrogen in our simulation box. The standard simulation parameters were as follows: time step=2fs, Berendsen temperature coupling=0.1ps at 300K, and cut off=0.85nm for both van der Waals and Coulomb interaction. The effect of the long range Coulomb interaction was accounted for by the particle mesh Ewald summation (PME) [12]. These conditions correspond to the NVT ensemble (constant number of particles, volume, and temperature). However, the difference between the Helmholtz and Gibbs free energies $\triangle(pV)$ is for our system negligible, therefore, we can also use equations for the NPT ensemble (constant number of particles, pressure, and temperature).

In the first stage of our simulations we tested several sets of different potential models. A summary of the molecular properties and force field parameterizations with their names and references is presented in Appendix B. For most simulations non-polarizable atoms were used because of the considerable saving of computer time. Nevertheless, we also tried polarizable models, described by a shell model in Gromacs (Drude oscillator), since for some systems polarizability can cause non-negligible effects [10].

We chose the SPC/E model [13] for water molecules. This decision was based on the calculations of the hydration free energy of a water molecule using the thermodynamic integration [14] method with standard parameters. The results for the SPC/E model together with other commonly used TIP3P and TIP4P [15] water models are compared with the experimental values in the Table 2.1. We also took into consideration water surface properties as the previously calculated surface tension [16, 17]. Two polarizable models were also tested, despite the fact that it took a considerable amount of computer time. Note that these polarizable models slightly underestimate the chemical potential of water: POL3 [18] and COS-G2 [19] models have hydration free energy of water only -22.5 kJ/mol and -23.0 kJ/mol, respectively.

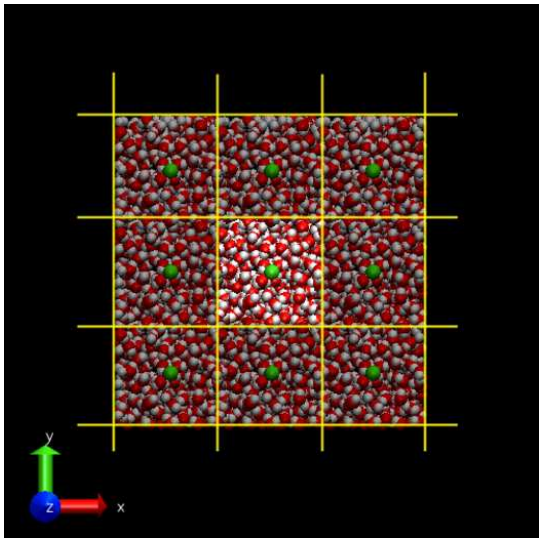

Figure 2.1: Periodic boundary conditions with a prismatic unit cell create an infinite water slab. (top view)

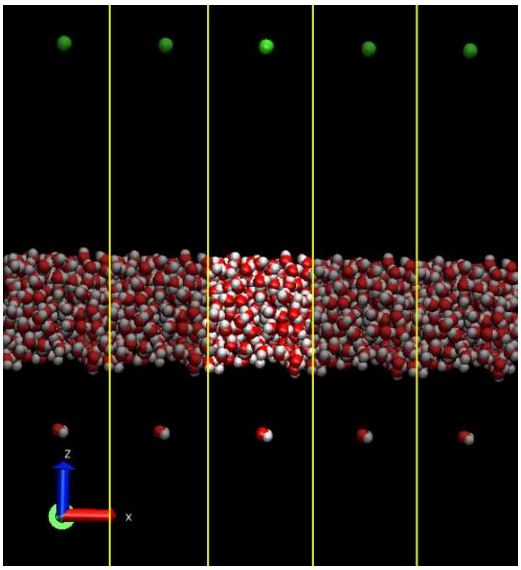

Figure 2.2: Periodic boundary conditions with a prismatic unit cell create an infinite water slab. (side view)

	SPC/E	SPC/E[1]	TIP3P	TIP3P[1]	TIP4P	Experiment
G_{solv} [kJ/mol]	-28.6	-24.3	-25.2	-20.1	-29.6	-26.3
γ [mN/m]	66		52.7		79	72

Table 2.1: The summary of the solvation energy G_{solv} and the surface tension γ of water models.

1) Values were calculated using PME, which can change the solvation energy since the lattice contribution to the free energy is not calculated.

2.2 Methods

There are several ways to obtain concentrations of solute molecules at the air/water interface. First approach is to simply run a very long simulation under ambient conditions and monitor the time averaged density of the solute in the simulation box. This method is called the Direct Sampling or Simple Sampling Method (SSM). Unfortunately, if there is a barrier or high-energetic region in the system, SSM would sample it poorly on the nanosecond time scale (this applies for example to the water bulk region for very hydrophobic molecules). To improve sampling in all regions an Umbrella Sampling Method (USM) was developed. This technique divides the system into a set of overlapping windows and performs separate simulation in each window. Artificial potentials can be applied which help the sampling to be more uniform. Once the simulations are done, the effect of the bias potential on the density profile has to be subtracted in each window. Finally, the data from all windows should be connected.

Indirect methods consist in calculation of the Gibbs free energy difference $\triangle G$ followed by a transformation to relative concentrations using the Boltzmann relation:

$$\frac{c_1}{c_2} = e^{-\frac{\triangle G_{12}}{RT}} \tag{2.2}$$

c_1 and c_2 are the concentrations in two states that differ by $\triangle G_{12}$, R is the universal gas constant, and T stands for temperature. It follows from Eq. 2.2 that it is equivalent to study the free energy profile instead of the concentration profile. The typical free energy and concentration profiles are shown in Figure 2.3, where the three important free energy differences are marked - the solvation (i.e., gas-to-liquid) free energy ΔG_{solv}, the gas-to-surface free energy difference ΔG_{gs}, and the surface-to-liquid free energy difference ΔG_{sl}. Only two of these values are independent, since $\Delta G_{solv} = \Delta G_{gs} + \Delta G_{sl}$.

The change of the free energy can also be obtained using Thermodynamic Integration (TI) [14]. In this method the Hamiltonian is slowly changed (keeping the system in equilibrium) from one state to another using a parameter λ. Using TI we can let the solute disappear and by a thermodynamic cycle we can obtain the free energy difference between the state with and without the molecule in the solvent.

$$\triangle G = \int_0^1 \left\langle \frac{\partial H(\lambda)}{\partial \lambda} \right\rangle_\lambda d\lambda \tag{2.3}$$

This simulation must be run for different positions of the solute in the water slab to obtain a free energy profile.

Another method to compute the Gibbs free energy change is the Constrained Method. It is a measurement of the force F_ξ acting on the solute

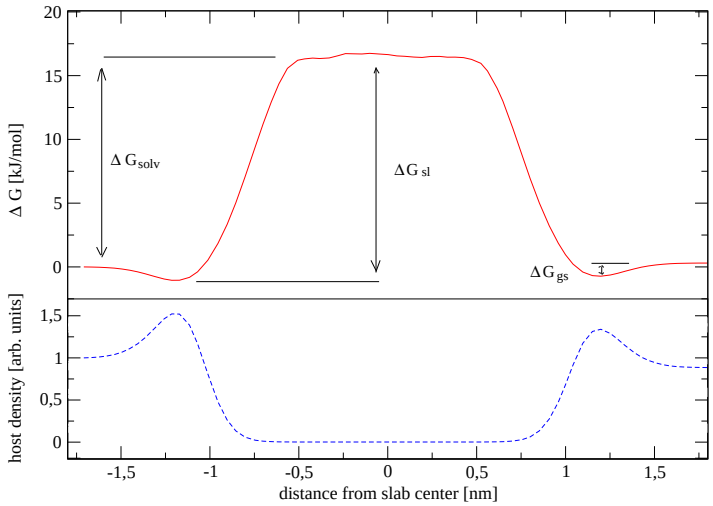

Figure 2.3: The free energy profile with marked important differences and the corresponding solute density profile (i.e., relative concentrations).

that is hold at a defined position with respect to the slab while the system is in equilibrium. Consequently, the force is integrated along the constrained (reaction) coordinate ξ to obtain the free energy profile (a typical one is shown in Figure 2.4). The free energy profile along a "reaction coordinate" (z-coordinate in our case) is the Potential of Mean Force (PMF). It is defined up to an arbitrary additive constant, which we choose to make the free energy difference equal to zero in the gas phase.

$$\triangle G_{ab} = -\int_b^a F_\xi d\xi \tag{2.4}$$

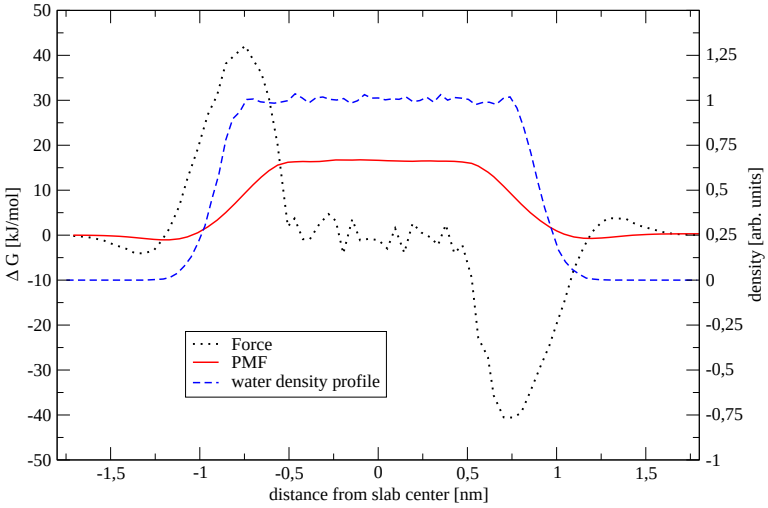

Figure 2.4: Typical profiles of the constrained simulation.

Both TI and Constrained Method need to keep the molecule in defined positions. This constraint can be applied in several ways. Freezing position means that the chosen coordinate is in each step changed to the previous value. Removing Motion of Center of Mass (RMCM) sets the velocity to zero every time step. The last possibility is to keep the molecule on a "z-spring" (i.e., apply a harmonic potential in the z coordinate).

Recently, two new methods appeared [20]. The first one is based on Jarzynski's expression [21, 22] that was further developed by Crooks [23, 24, 25]. This expression connects the Gibbs free energy difference $\triangle G$ with the non-equilibrium works W_τ(at time τ) by averaging them over all trajectories:

$$e^{-\frac{\triangle G}{RT}} = \overline{e^{-\frac{W_\tau}{RT}}} \tag{2.5}$$

$\triangle G$ between two reversible states is equal to equilibrium (i.e., infinitely slow) work that is required to switch between these states. However, to get this work from simulations requires long runs which is computationally expensive. $\triangle G$ can be accurately estimated using Eq. 2.5 from the non-equilibrium work W_τ for switching between the two states within a finite time τ even if the system is far from equilibrium like in fast computer simulations or in some experiments, such as micromanipulation of molecules.

The second new method is called Adaptive Biasing Force method (ABF). This method improves sampling of the system, even if high energy barriers are present, and no a priori estimated biasing potential is known. An external force F_B is applied on the solute and it is equal in size and opposite in sign to the running average of the n last acting forces $F_{\xi,i}$:

$$F_B = -\frac{\sum_{i=1}^{n} F_{\xi,i}}{n} \tag{2.6}$$

2.3 Henry's Law

The ratio between concentration in the liquid and in the gas phase can be compared with the experimental Henry's law constant. The Henry's law constant can be defined as the concentration of host molecules in the liquid divided by their partial pressure in the gas phase [26]:

$$k_H = \frac{c_l}{p_g} \tag{2.7}$$

The Henry's law constant can be rewritten in a dimensionless form as the ratio between the concentrations in the liquid and in the gas phase:

$$k_H^{cc} = \frac{c_l}{c_g}, \tag{2.8}$$

where c_l and c_g are concentrations in the liquid and in gas phases and k_H^{cc} is the concentration Henry's law constant. If we consider ideal gas conditions and use the Equation (2.2), we get a simple relation between these two constants and the solvation Gibbs free energy of the molecular species at infinite dilution:

$$k_H^{cc} = k_H \cdot RT = e^{-\frac{\triangle G_{solv}}{RT}} \tag{2.9}$$

where, k_H is the Henry's law constant, R is the universal gas constant, T stands for temperature, and G_{solv} is the solvation Gibbs free energy. It should be emphasised, that the standard solvation free energies (at $p_0 = 1atm$ gas pressure and $c_0 = 1M$ concentration) differ from those corresponding to a single gas molecule (i.e., pertinent to the present simulations) by a factor $RT \ln\left(RT\frac{c_0}{p_0}\right)$, which at standard conditions amounts to 1.9kcal/mol [27]. The values of Henry's law constant were taken from a compilation by Sander[28].

Chapter 3

Benchmarking

3.1 Choosing the optimal method

We chose the Constrained Method with the z-spring as the most suitable one for our purpose. Since it is an indirect method we compared it with the direct SSM approach. In spite of the fact that the SSM method can efficiently sample only certain regions of the system, it verifies large part of the data from the Constrained Method with the z-spring (Fig. 3.5 and 4.11). The Umbrella Sampling is also a direct method, but it requires a good guess of the biasing potential to achieve an efficient sampling, moreover, results from different windows have to be connected. Overlapping parts are usually matched using the least square method. However, a better method improving the sampling, the ABF method, was developed and we tested it as well.

Other methods described in the previous chapter suffer from the difficulty to keep the solute molecule at a desired position with respect to the water slab. There are several possibilities without using the z-spring, consisting of combination of freezing and RMCM. Freezing the z-coordinate should not be used for the slab because it holds all molecules in their z-positions and diffusion is compromised. Using RMCM for the solute causes the "trunk effect" described in the following paragraph. The last combination (RMCM applied to the slab and freezing the z-coordinate of the solute) leads to massive evaporation of water molecules. This happens as follows: first, as the slab gets closer to the solute molecule, its surface deforms a bit towards the attracted solute. Since the RMCM is applied on the slab a small ventricle appears on the side opposite to the solute. As the process continues the slab elongates in the z-coordinate and finally breaks into pieces. Therefore, using the spring is a necessary step. We can also use it to measure the force acting on the spring $f(z')$ and then employing the following formula calculate the PMF.

$$\triangle F\left(z\right) = -\int_{z_0}^{z} f\left(z'\right) dz' \tag{3.1}$$

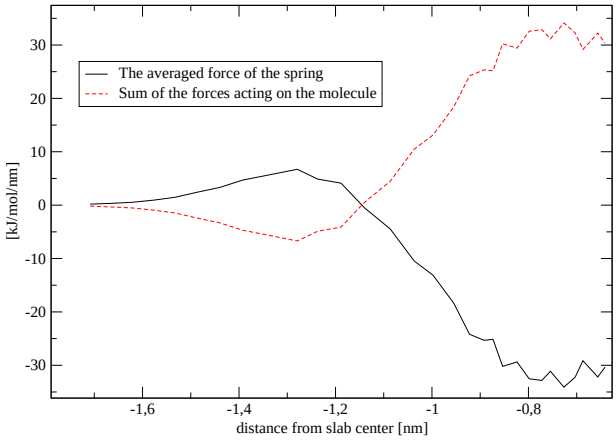

Figure 3.1: The profiles of averaged force of the spring and averaged force acting on the solute are the same except the sign.

Note, that in a general case the formula for calculating the unconstrained free energy change from constrained simulations is more complicated (Eq. 3.2) [29], because the constrain can influence the other degrees of freedom of the system.

$$\triangle F\left(\xi\right) = -\int_{\xi_0}^{\xi}\left(f\left(\xi'\right) + kT\frac{\partial log\left|J\right|}{\partial\xi'}\right)d\xi', \tag{3.2}$$

where k is the Boltzmann constant, T stands for temperature, ξ is the generalized reaction coordinate along which the constrain is applied, and J is the Jacobian of the transformation from Cartesian to generalized coordinates.

RMCM of the solute restricts its freedom in the xy plane. This causes the so called "trunk effect" which one can see in the following illustrative snapshots taken from a simulation.

a) 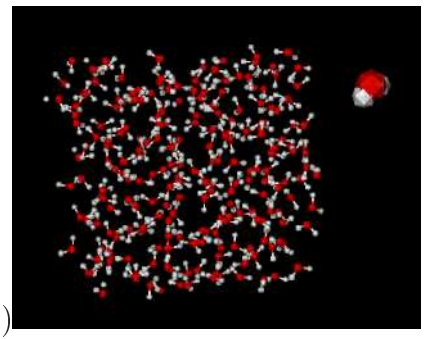 b) 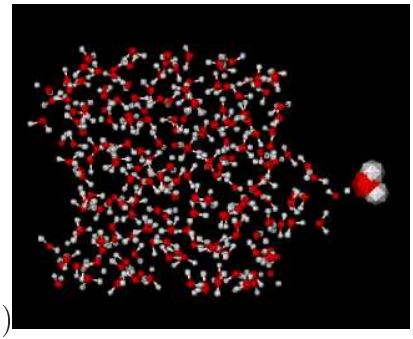

Figure 3.2: a) Water molecule close to the water surface with possibility to move in xy plane. b) Water molecule close to the water surface with RMCM.

The "trunk effect", i.e. an artifact, where water molecules are dragged with the solute into the gas phase, changes the PMF as shown in Fig.

3.3. The same force as acting on the z-spring at the surface is present with RMCM already about 0.1 nm above it (towards the gas phase).

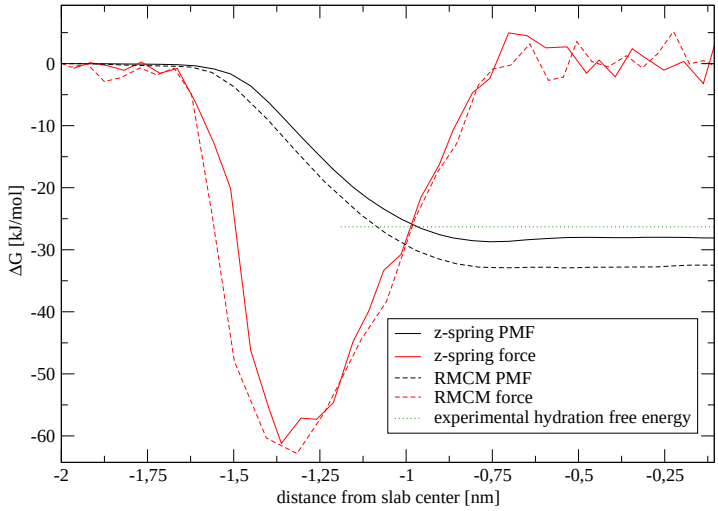

Figure 3.3: The PMF and force profiles for water molecule pulled into the water slab. (two methods)

The non-equilibrium method was compared with the ABF method previously [20]. The non-equilibrium method performs well but not better than the ABF method. Its relative inefficiency was due to the broad non-equilibrium work distribution which is difficult to sample.

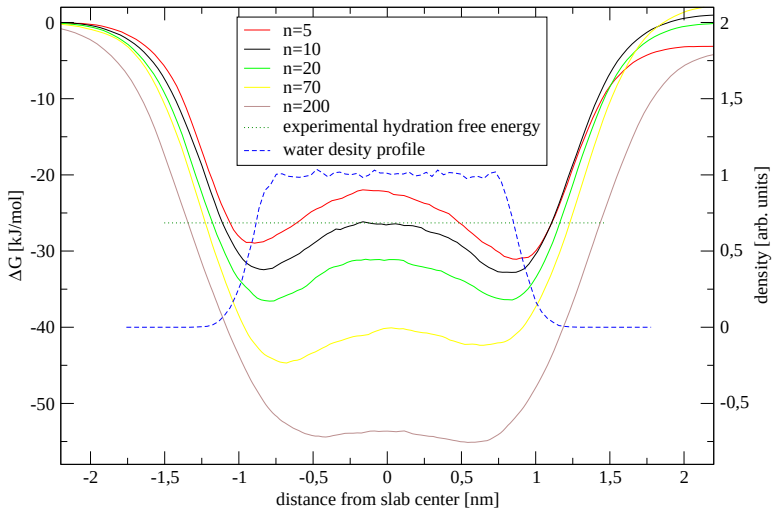

Figure 3.4: The PMF for the ABF method using different n.

The results of the ABF method depend on the number of averaged forces n in the Eq. 2.6. It can be easily seen that if $n = 1$ there is no final force acting on the solute, so it is moving with a velocity corresponding to its temperature, whereas if $n = \infty$ the biasing force is zero. We did simulations for several different values n and the resulting PMFs are

shown in Fig. 3.4. For the small n there is barrier in the middle of the slab which is caused by the non-equilibrium work: since the solute molecule is only weakly affected by other molecules it goes through the slab fast pushing thus the system out of equilibrium. For bigger n the system is kept in equilibrium, but since the biasing force causes the solute to leave the surface slowly the "trunk effect" appears.

The best method for obtaining the PMF turned out to be the constrained method using a spring for constraining the z-position (perpendicular to the interface). This approach was tested and verified against the direct SSM method on ozone solvation energy which is close enough to zero, so a long simulation can sample the whole box rather well (for the corresponding density profiles see Fig. 3.5).

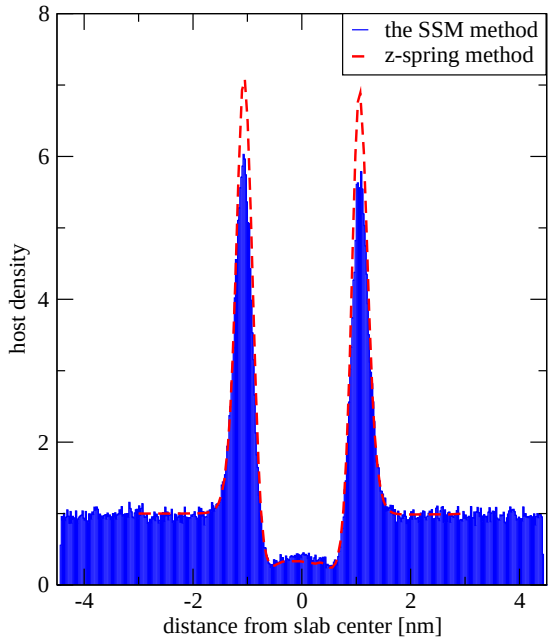

Figure 3.5: Host density profiles for ozone molecule by two methods that are compared.

Based on the quantitative agreement with the direct SSM method and with experiment we chose this z-spring constrained method for obtaining the PMFs for all the gases under study. To get a smooth PMF profile we used 80 cycles of sampling and pulling simulations. During each of the 1.5ns sampling periods the equilibrium length of the spring was kept constant and the force was monitored and averaged over time. The pulling phase, during which the equilibrium length of the spring was changed by 0.05nm, took 20ps .

Simulations of ions represent a different situation and considerable challenge. It is well known that, the hydration free energy of ions is very large compared to neutral molecules. We tested the Constrained Methods, but the ion always became covered by few vaporised water molecules

after being placed into the gas phase. So the measured force is the force on the ion-water cluster rather than that on the bare ion. Moreover, if we pulled the ion out of water it took with it strongly attracted water molecules, so again we did not get the hydration energy of the bare ion. As a matter of fact, no matter what method we used, we could get free energies pertinent to the bulk and surface only, but not that of the bare gas phase ion.

3.2 Parameters dependence

We performed many simulation in order to study the change of the PMF with respect to a change of parameters. We divided all parameters in two groups: "MD parameters" and "topology parameters".

MD parameters included the time step, temperature coupling, length of simulation, initial configuration, force constant, etc. We can conclude that if the system was in equilibrium during the measurement phase, changes of these parameters within reasonable margins did not cause significant changes of the PMF (Fig. 3.6).

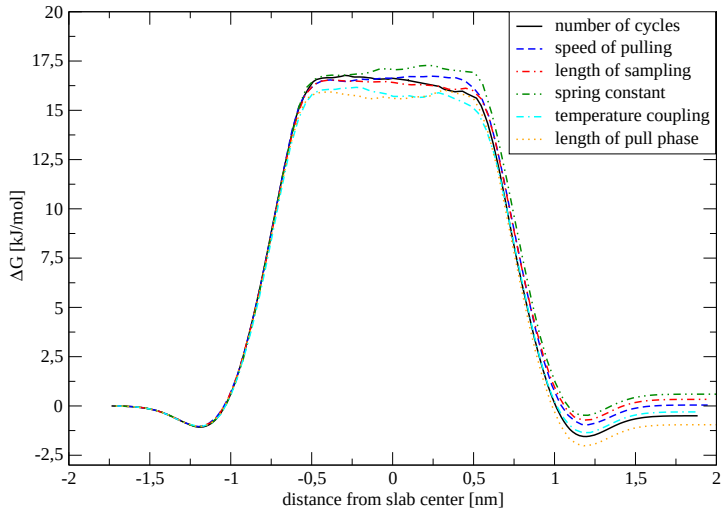

Figure 3.6: The PMF profiles for nitrogen molecule with different MD parameters. It also shows convergence of parameters and good equilibration of the system.

Due to the symmetry of the slab system, the PMF should be symmetric as well. However, this is never exactly true, so the difference between the two ending values of the PMF indicates the size of the error caused by passage of the solute through the slab. We compared the ΔG_{gs} from the left and right side from simulations with different MD parameters and we got practically the same numbers (Table 3.1). This implies, that the profile was only slightly shifted inside the slab, where many collisions occurred and it was difficult to establish perfect equilibrium.

	1	2	3	4	5	6
Left ΔG_{sl} [kJ/mol]	-1.074	-1.049	-1.035	-1.049	-1.018	-1.037
Right ΔG_{sl} [kJ/mol]	-1.052	-1.000	-1.057	-1.072	-1.057	-1.072

Table 3.1: Comparison of the "right" and "left" ΔG_{sl} from the PMF for different MD parameters. (1-number of cycles, 2-speed of pulling, 3-length of sampling, 4-spring constant, 5-temperature coupling, 6-length of pull phase)

Topology parameters include the geometry, charge distribution, and Lennard-Jones parameters of the solute. Changes of these parameters caused significant changes of the PMF. The influence of the charge distribution was dependent on the order of the multipole expansion (i.e., the change of the dipole was more important than the change of the quadrupole). The corresponding changes of the PMF are demonstrated in Figure 3.7 and in the Table 3.2.

We also studied the PMF dependence on the temperature change of ±20K from the reference value. This was 300K and the changes were negligible.

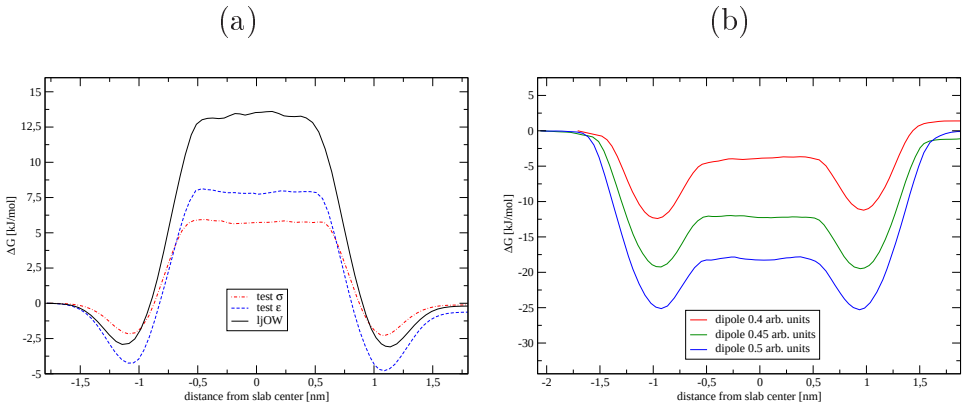

Figure 3.7: The change of the PMF caused by (a) the change of σ and ε is on the left side (oxygen molecule), (b) by dipole (hydroxyl radical). Legends correspond to molecular models, which are described in detail in Appendix B.

Ozone	ΔG_{solv}	ΔG_{sl}	ΔG_{gs}
ljOW	13.60	-2.92	16.52
test σ	5.73	-2.17	7.90
test ε	7.97	-4.24	12.21

HO radical	ΔG_{solv}	ΔG_{sl}	ΔG_{gs}
ljOW	-5.10	-12.55	7.45
OW-45	-12.17	-19.24	7.07
OW-50	-18.27	-25.13	6.84

Table 3.2: Change of the PMF caused by topology parameters in kJ/mol. Employed models are described in details in Appendix B.

Effects of the parameters of neutral molecules on the PMF are schematically summarized in Table 3.3.

		$\Delta\Delta G_{solv}$	$\Delta\Delta G_{sl}$	$\Delta\Delta G_{gs}$
MD parameters		small if the system is equilibrated and the pull is slow		
Dipole ↑		Large ↓	Large ↓	Small ↓
Quadrupole ↑		Small ↓	Small ↓	Small ↓
LJ parameters	σ ↑	Large ↓	Large ↑	Large ↑
	ε ↑	Large ↓	Large ↓	Large ↓
Temperature ↑		Very small ↑	Very small ↑	Negligible

Table 3.3: Summary of the PMF changes caused by different parameters.

Chapter 4

Results

There are several force field models available for most of the investigated molecules and each parametrization is suitable for different situations and purposes. In our case, all models were examined with respect to the hydration free energy and compared with experimental values. For further simulations, we chose the best model or in some cases a new better parametrization had to be developed by a combination of existing models or by a slight change of the atomic charges. All PMF results for different parameterizations are summarized as graphs in Appendix D. In the following we present and discuss our "best" simulation results and compare them to solvation free energies derived from the experimental Henry's law constant taken from Ref. [28].

4.1 Hydrophobic molecules N_2, O_2, and O_3

The PMFs of the nitrogen molecule for non-polarizable and polarizable force fields are presented in Figure 6.1. Both models reproduce well the solvation free energy of +10.5kJ/mol and the two free energy profiles are very similar to each other. The PMF surface minima of about 4kJ/mol correspond to an enhanced concentration of nitrogen at the water surface. This surfactant activity of the dominant atmospheric gas is in agreement with the small decrease of surface tension of water with the increase of atmospheric pressure (by about 0.1 $\frac{mN}{m\,atm}$) [9]. The surface minimum is slightly more pronounced for the polarizable force field, which is due to an additional stabilization via polarization interaction in an inhomogeneous dielectric environment of the air/water interface [30].

The PMF of O_2 is similar to that of N_2. The employed model satisfactorily reproduces the experimental solvation free energy of +8.5kJ/mol (Fig. 4.2). The surface minima are over 2kJ/mol deep. This means a 240% oxygen increase the water surface at an ambient temperature. A very weak barrier (of less than 1 kJ/mol) between the aqueous bulk and the surface region seems to develop at the PMF. This behaviour is con-

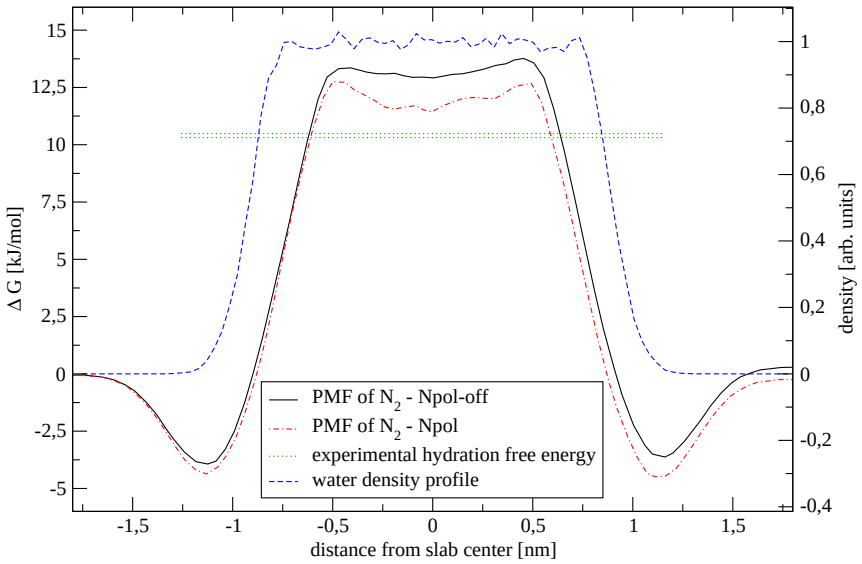

Figure 4.1: The final PMF for the nitrogen molecule. Employed forcefields are described in detail in Appendix B.

sistent with previous studies [31]. However, the barrier height is within the error of the calculation that was estimated from the noise and the asymmetry of the PMF curve with respect to the center of the water slab.

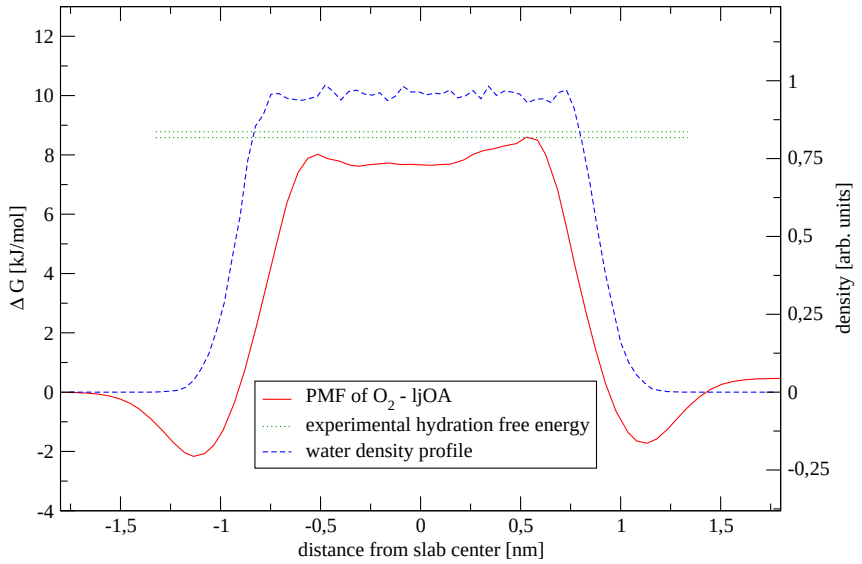

Figure 4.2: The final PMF for the oxygen molecule. Employed forcefield is described in detail in Appendix B.

Ozone is less hydrophobic than nitrogen and oxygen. The employed forcefield reproduces well the experimental solvation free energy of +3-4kJ/mol. As in the previous cases the surface minima develop with an

even larger depth of 5kJ/mol (Fig. 4.3). This means about roughly a seven-fold enhancement of O_3 concentration at the water surface at 300K. This surfactant behaviour is in agreement with the previous computational results on ozone uptake [32]. A very weak barrier between the surface and the bulk region appears, but it is again below the estimated error.

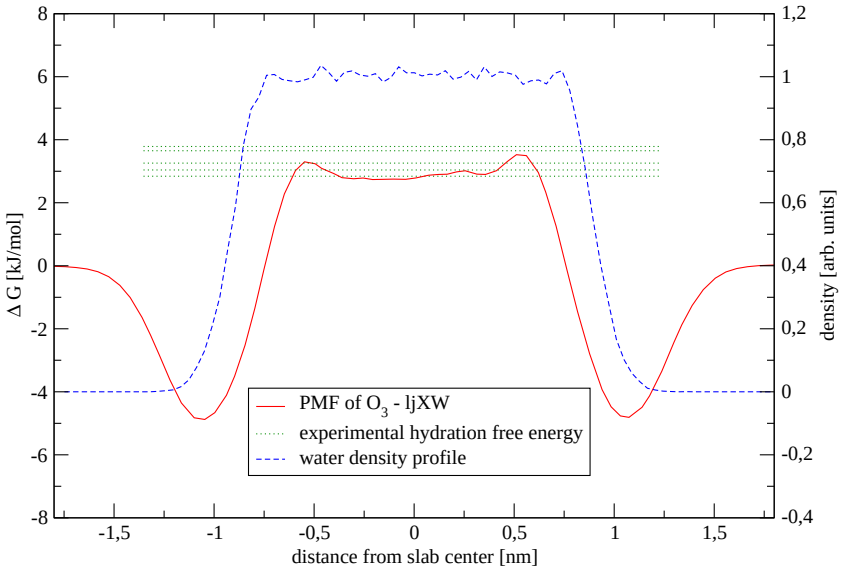

Figure 4.3: The final PMF for the ozone molecule. Employed forcefield is described in detail in Appendix B.

4.2 Hydrophilic molecules and radicals OH, H_2O, HO_2, and H_2O_2

For hydrophilic gases the solvation free energy is negative (i.e., the free energy in water is lower than in the air). This is true for all the above species, moreover, the hydration free energy of the peroxide and hydroperoxy radical is even larger than that of a water molecule.

The employed forcefields (both polarizable and non-polarizable) for OH radical reproduce the experimental solvation energy of about -16kJ/mol reasonably well (Fig. 4.4). The PMF develops very deep surface minima of about 6kJ/mol, which corresponds to a ten times enhanced concentration of hydroxyl radical at the air/water interface compared to the aqueous bulk. Our results are in agreement with previous dynamical studies of the uptake of OH radical at water surface [32, 33].

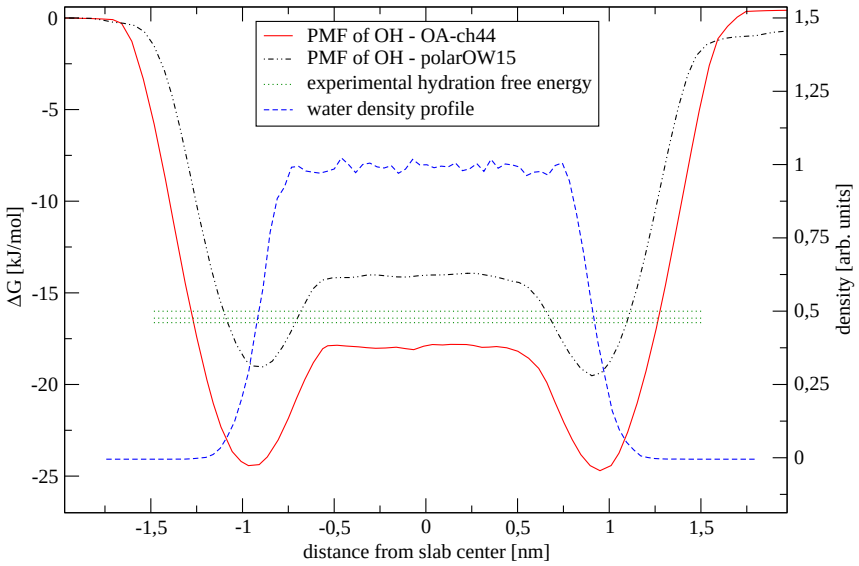

Figure 4.4: The final PMF for the hydroxyl molecule. Employed forcefields are described in detail in Appendix B.

The hydration free energy for water obtained from our simulations reproduces its chemical potential of -26.3kJ/mol well [27] (Fig. 4.5). There are no perceptible (above statistical and systematic error) surface minima at the air/water interface in the PMF of H_2O. This is consistent with the fact that water is obviously not a surfactant on water. [34].

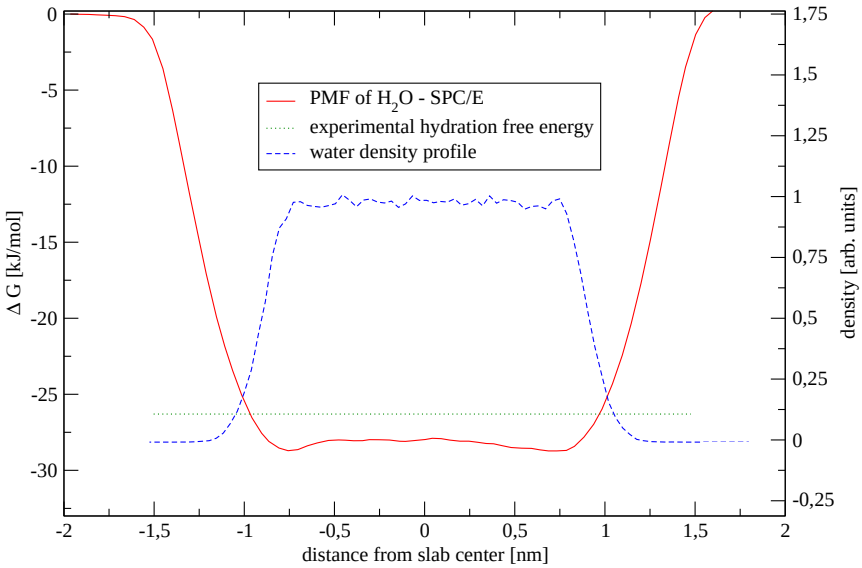

Figure 4.5: The final PMF for the water molecule. Employed forcefield is described in detail in Appendix B.

Both simulations for the HO_2 radical and H_2O_2 reproduce the experimental solvation energies of -25.7 to -35.5kJ/mol and -35.7 to -37.5kJ/mol,

respectively (Fig. 4.6 and 4.6). Somewhat unexpectedly, PMF minima at the air/water interface are observed, despite the fact that both gases are more hydrophilic than water vapor itself. The depths of these minima are about 3 kJ/mol for hydroperoxy radical and 1.5kJ/mol for hydrogen peroxide.

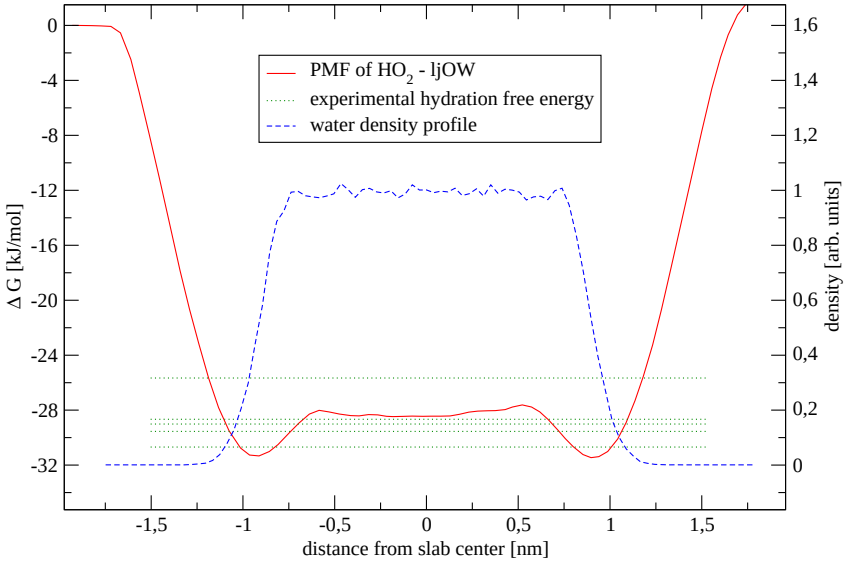

Figure 4.6: The final PMF for the hydroperoxy radical. Employed forcefield is described in detail in Appendix B.

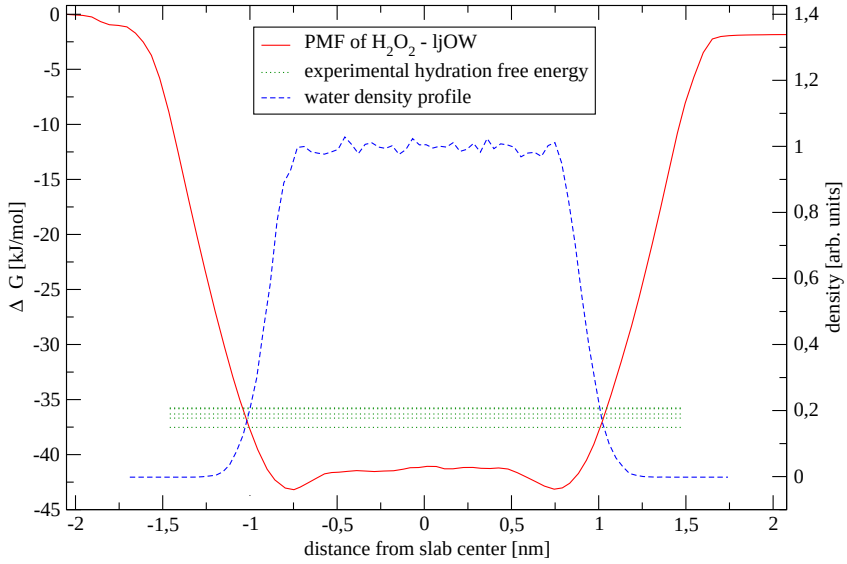

Figure 4.7: The final PMF for the hydrogen peroxide molecule. Employed forcefield is described in detail in Appendix B.

4.3 F^-, OH^-, Na^+, H_3O^+, and $H_5O_2{}^+$ Ions

Experimental ion hydration free energies are not reproduced by PMF calculations for reason explained in detail in chapter 3.1. Also the right end of the PMF curve usually lies below zero since the ion has usually more waters on way out of the slab than into it. There are no minima at the surface for the small ions as expected for non-polarizable simulations [10].

Somewhat surprising are the observed surface minima for the bigger $H_5O_2{}^+$ ion which is the Zundel form of the hydrated proton. The minima are likely due to the size of the molecule which leads to the big entropy change during solvation and an energy penalty for complete solvation (hydrophobic effect). The size also causes the little shift of the right hand side minimum (on the way out of the slab), since our slab is so small that the big molecule, dragging a lot of molecules with it, is able to slightly move the whole slab.

Because of the difficulties of the PMF calculations for ions (see chapter 3.1), the simulations finished at testing phase and none of the forcefields was chosen, therefore, the results are shown only in Appendix D.

4.4 Surface analysis

The surface analysis was made to find out the physical reasons for the development of surface minima in the PMF, particularly for very hydrophilic molecules. Several detailed simulations at the air/water interface were aimed a monitoring interaction energies and dipole orientation. The "entropy" profile was calculated as the PMF minus the Lennard-Jones and Coulomb energy contributions.

Hydrophobic molecules are represented by O_2. The oxygen molecule has no dipole, so attractive Lennard-Jones interaction was expected to dominate. This was confirmed by the simulations (Figure 4.8). The minima at the surface were caused by attractive the Lennard-Jones interaction energy that first increased faster than entropy term, when moving from the gas phase. After a short distance, however, the situation reversed, which leads to the hydrophobic part of the PMF in the aqueous bulk. Similar analysis was also made for the other hydrophobic molecules.

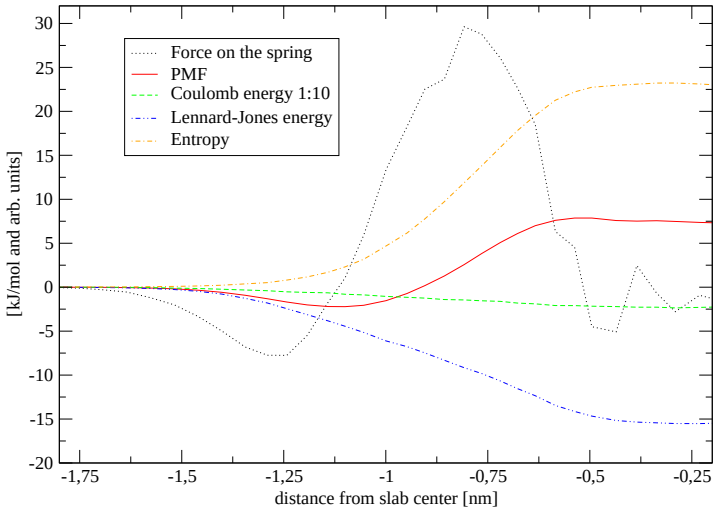

Figure 4.8: The profiles of interaction energies and the PMF for oxygen molecule pulled to the water slab.

Hydrophilic molecules were studied in more detail. First, we looked at the dipole orientation. As shown in Figure 4.9, the dipole orientation with respect to the z-coordinate was increasing and decreasing according to the distance from the water surface with no preference of the opposite orientation. So the HO_2 dipole was not behaving with respect to the dipole layer at water surface, but rather to its local environment. We observed this effect also for OH radical with polarizable forcefields.

The profiles of the interaction energies seem to differ for hydrophobic (Fig. 4.8) vs. hydrophilic (Fig. 4.10) molecules. The first difference for the hydrophilic species is in the Lennard-Jones interaction energy, which is mainly repulsive for hydrophilic molecules. The second difference is that the Coulomb attractive interaction plays a very important role and its combination with entropy causes the surface minima. This seams to be a generic effect for all tested hydrophilic molecules, radicals, and even for the larger ion $H_5O_2^+$. The stronger Coulomb attraction probably also causes a slight shift of the surface minima towards the aqueous bulk compared to the hydrophobic molecules.

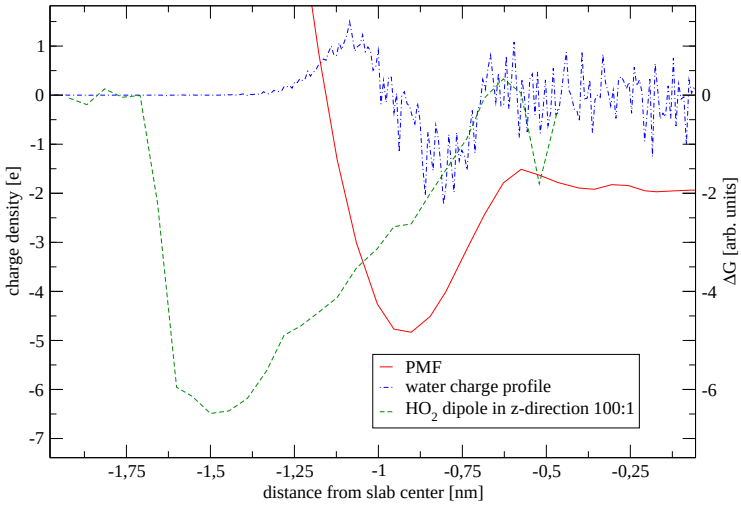

Figure 4.9: The charge distribution profile of water interface and dipole orientation of HO_2 (the preferred orientation is with hydrogen pointing to the surface).

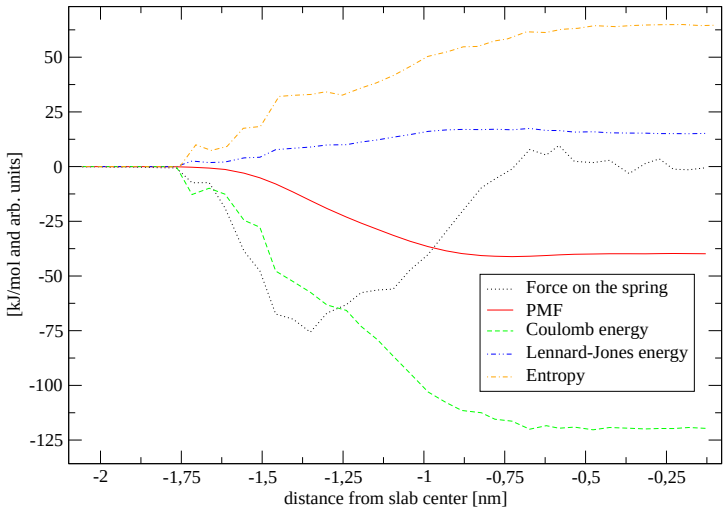

Figure 4.10: The profiles of interaction energies between water and peroxide molecule pulled to the water slab.

Another issue is the validation of the calculated surface minima by direct calculations. By comparison to direct results (SSM) we demonstrate in Figure 4.11 the fact, that the z-spring method did not artificially cause the PMF minima at the surfaces.

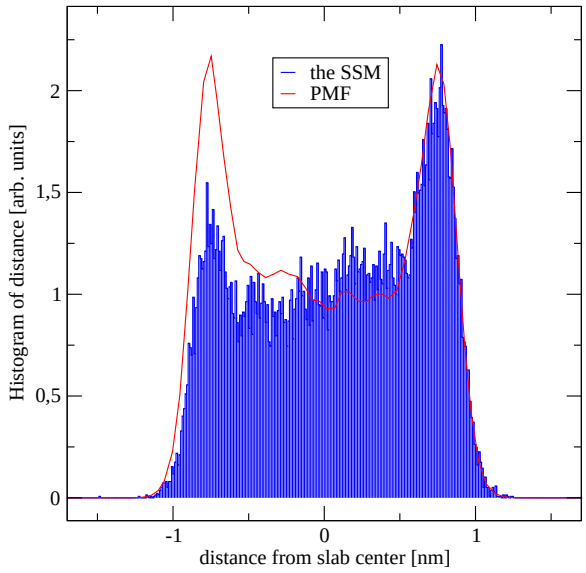

Figure 4.11: Host density profiles for H_2O_2 in the water slab obtained from different methods (the non-perfect symmetry of minima at the surface in sampling simulation was caused by the finite length of the simulation).

Another effect is the occurrence of the tiny subsurface barrier, which is explicitly visible, e.g., for O_3. This barrier with height lower than 1kJ/mol increases when the pulling speed is doubled (Fig. 4.12). For this reason we deduce that the barrier is largely caused by non-equilibrium work and is, therefore, to a large extent artificial.

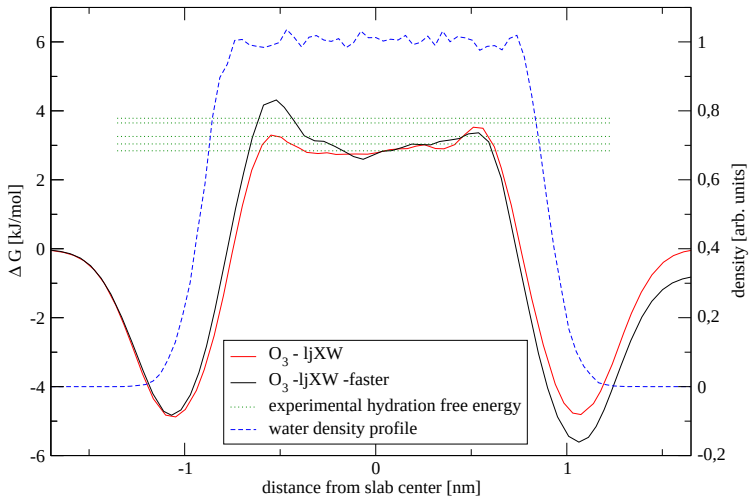

Figure 4.12: The profiles of ozone molecule pulled to the water slab with normal and double speed.

4.5 Atmospheric implications

The increased concentration of inorganic molecules at the air/water interface is important for reactions at the surfaces of fog and cloud droplets. Over the last decade, several atmospheric reactions of inorganic species have been recognized to occur at the interfacial region [3, 35, 36, 37, 38]. Our simulations show that atmospherically important molecules are enhanced at the water surface. A major type of atmospheric reactions in the troposphere is oxidation. The hydroxyl radical and ozone are the main oxidants during the day, while ozone is present and, therefore, active also at night.

The enhanced concentrations of OH and O_3 at the surfaces of aqueous atmospheric particles may play a significant role in heterogeneous oxidation processes. This is particularly true for molecules that are also enhanced at the air/water interface such as alcohols and polycyclic aromatic hydrocarbons (PAH) of intermediate size (smaller PAH are predominantly present in the gas phase). Higher concentrations of PAH and alcohols occur in air in urban areas or during biomass burning events. In recent field studies oxidation of methanol has been observed to be much more rapid than predicted from the gas and bulk chemistry. Tabazadeh and coworkers suggested that it was due to heterogeneous processes [39]. These processes can also be behind the unusually fast oxidation of anthracene at the air/water interface that has been measured by Donaldson and coworkers [40]. The increased concentration of ozone at the air/water interface also leads to a higher production of hydroxyl radicals and its precursors such as H_2O_2 at the interface [1]. Thus the oxidation capacity on the droplet surfaces is large, however, it can be influenced also by other factors such as the surface coverage by organic species.

Surface enhancement is rather weak for some of the studied molecules. For example, hydrogen peroxide surface concentration is increased only by 50 percent compared to the liquid phase. This is consistent with the experiment [41], where the surface reaction of H_2O_2 and SO_2 was not important compared to the liquid phase, in spite of the existence of a SO_2 surface complex. Note, that peroxide is one of the main atmospheric oxidants in bulk water.

Chapter 5

Conclusion

We studied the behaviour of selected molecules and ions at the air/water interface by means of molecular dynamics simulations. In order achieve this goal a system consisting of a water slab and a solute species was employed. We investigated different simulation methods for obtaining the concentration and free energy profiles of the solute moving from the gas phase into the aqueous phase across the air/water interface. We participated on the development and implementation of several approaches and we explored the advantages and disadvantages of the various methods. On one hand, the main observed problems with indirect methods consisted in holding the desired distance between the solute and the water slab and avoiding the so called "trunk effect". On the other hand, in the case of direct methods the difficulties arose from inefficient sampling of high energy regions. We chose the indirect Constrained Method employing a z-spring (i.e., using a constraining harmonic potential in the coordinate perpendicular to the air/water interface) as the most suitable method. Using this method we calculated the free energy profiles across the air/water interface, i.e., the Potentials of Mean Force, by measuring the forces acting on the solutes.

We found generic dependencies in the PMF changes on various simulation parameters (see Table 3.3). In each case, we selected among the existing molecular models according to the best agreement with the experimental hydration free energy of the solute. When none of the existing models was satisfactory we developed a new one. The hydration free energies derived from the experimental Henry's law constants for neutral molecules were then well reproduced. For ions we were not able to obtain gas phase free energy values since they remained covered with water vapour due to strong ion-water interactions. Nevertheless, these simulations gave us information about ions in the bulk water and at the interface. We used primarily non-polarizable parametrization because of the unavailability of polarizable models in most cases and because of high computational cost of polarizable calculations. However, we kept in

mind that the surface stabilization of the host species might actually be somewhat underestimated due to the lack of polarizability.

According to our simulations the enhanced concentration of molecules at the air/water interface is a generic effect present for all neutral species (both hydrophobic and hydrophilic) with the exception of water vapor itself. The surface analysis was made and the changes in interaction energies at varying distances from the surface was investigated. The Lennard-Jones interaction is the leading force for creating minima at the air/water interface for hydrophobic molecules, while the Coulomb interactions overwhelm all other interactions in the case of hydrophilic species. The increase of population of the solute species at the water surface compared to the second most populated region (gas phase or aqueous bulk) is ranging from a factor of 2 (e.g., for H_2O_2) to a factor of about 10 (e.g., for OH).

The results from the PMF converted to the concentration profiles assuming ambient conditions are summarized in Table 5.1. The investigated molecules are shown together with their aqueous bulk concentration values, the highest surface values, and the surface averaged value (all normalized to the air values). The surface enhancement of atmospherically relevant gases has important consequences for heterogeneous chemical processes occurring on aqueous atmospheric particles. In particular, the increased concentration of ozone and hydroxyl radical at the air/water interface may be responsible for recently measured faster oxidation of alcohols and polycyclic aromatic hydrocarbons than predicted from the gas phase and aqueous bulk chemistry [39, 40].

Finally, we note that a condensed version of this work has already been communicated via a full-scale research article published in the Journal of Physical Chemistry A [42].

	Gas phase	Aqueous bulk	Aqueous surface highest value	Aqueous surface averaged value	Width of the interfacial peak [nm]
N_2	1.0	0.0087	4.9	3.21	0.57
O_2	1.0	0.046	2.4	1.44	0.57
O_3	1.0	0.33	7.1	3.17	0.83
OH	1.0	1100	11000	8800	0.69
H_2O	1.0	75000	75000	75000	0.00
HO_2	1.0	90000	290000	141000	0.44
H_2O_2	1.0	17000000	34000000	20200000	0.37

Table 5.1: Aqueous bulk concentrations and their highest and averaged values in the interfacial region (all with respect to the gas phase value) for the investigated atmospheric gases

Chapter 6

Appendices

6.1 Appendix A - Interatomic interactions

Interactions between atoms and molecules depend on their type and mutual separation. Generally speaking, neutral molecules are strongly repelling each other at very short distances and weakly attracting each other at larger separation. To describe this behaviour one often employs the Lennard-Jones potential:

$$V_{LJ}(r) = 4\varepsilon\left(\left(\frac{\sigma}{r}\right)^{12} - \left(\frac{\sigma}{r}\right)^{6}\right) = \frac{C_{12}}{r^{12}} - \frac{C_6}{r^6}, \tag{6.1}$$

where r is a distance between interacting atoms and ε, σ, C_{12}, C_6 are constants. There is also the Coulomb interaction between atoms bearing a full or partial charges described by the formula:

$$V_c(r) = \frac{1}{4\pi\varepsilon_0}\frac{q_1 q_2}{\varepsilon_r r}, \tag{6.2}$$

where r is the interatomic distance, q stands for atomic charges, ε_r is the relative permittivity and ε_0 is the permittivity of vacuum. Since V_c decreases only as $\frac{1}{r}$ cutting off the interaction, required for saving computer time, causes error. A method for correcting the error is the Ewald summation [43]. It is based on a summation of charges in a periodic structure in the reciprocal space. A particle-mesh Ewald (PME) approach improves the computational efficiency of the method [12].

The bond stretching between two atoms in a molecule is represented by a harmonic potential:

$$V_b(r) = \frac{1}{2}k\left(r - r_0\right)^2, \tag{6.3}$$

where k is the force constant and r_0 stands for the equilibrium distance. A similar potential is employed for bending interactions:

$$V_a(r) = \frac{1}{2}k(\alpha - \alpha_0)^2, \tag{6.4}$$

where α is bending angle. For molecules with more than three atoms the dihedral potential is applied:

$$V_d(r) = k_d(1 + cos(n\theta - \theta_0)), \tag{6.5}$$

where θ is angle between planes defined by first and last trios of atoms.

Polarizability is implemented in Gromacs [11] using the shell model of Dick and Overhouser [44]. A charged shell particle which represents the electronic degrees of freedom is connected to an atom by a spring. Potential energy is minimized every time step via changing the length of the spring.

6.2 Appendix B - Molecular parametrization

H_2O

There are many models for water available, which demonstrates its importance, as well as difficulties in parametrization. We used three rigid water models SPC/E [13], TIP3P [15], and TIP4P [15] already implemented in Gromacs [11] and two polarizable models POL3 [18] and COS-G2 [19]. The forcefield parameters are summarized in the following table.

		σ [nm]	ε [kJ/mol]	charge [e]
SPC/E	H	0.0000	0.0000	0.4238
	O	0.3166	0.6501	-0.8476
TIP3P	H	0.0000	0.0000	0.4170
	O	0.3151	0.6359	-0.8340
TIP4P	H	0.0000	0.0000	0.5200
	O	0.3154	0.6485	0.0000
	D[a]	0.0000	0.0000	-1.0400
POL3[b]	H	0.0000	0.0000	2.3650
	O	0.3204	0.6527	-2.7300
COS-G2[c]	H	0.0000	0.0000	0.5265
	O	0.3196	0.7611	0.0000
	D[a]	0.0000	0.0000	6.9470

[a] is an auxiliary atomic site made for better reproduction of charge distribution

[b] polarizable model [18] with polarizability of 0.528Å^3 on oxygen and 0.170Å^3 on hydrogen

[c] polarizable model [19] with polarizability on dummy atom of 1.2555Å^3

N_2

Nitrogen molecule consists of the two nitrogen atoms separated by an equilibrium distance of 0.1098nm. Three point charges are distributed such as to reproduce the molecular quadrupole [45] (in the middle between the negatively charged nitrogen atoms a dummy atom with a positive charge is placed).

	σ [nm]	ε [kJ/mol]	quadrupole [DÅ]
2CLJQ[a]	0.3321	0.2900	1.4397
G-library[b]	0.2976	0.8767	1.4397
ljX[c]	0.3149	0.5042	1.4397
Npol[d]	0.4201	0.8256	
Npol-off[e]	0.4201	0.8256	

[a] parametrization from [45]

[b] Lennard-Jones parameters from Gromacs forcefield

[c] combination of parametrization [a] and [b]

[d] polarizable model [46] with polarizability 0.40367Å^3 on nitrogen atoms and 0.42704Å^3 on dummy atom in centre

[e] same model as d model [46] but with polarizability turned off

O_2

The parametrization for oxygen is similar to that for the nitrogen molecule. The interatomic distance is 0.121nm and three point charges are used to create the molecular quadrupole [45].

	σ [nm]	ε [kJ/mol]	quadrupole [DÅ]
ljOW[a]	0.3166	0.6502	0.8081
ljOA[b]	0.2955	0.8490	0.8081

[a] Lennard-Jones parameters for SPC/E water oxygen

[b] Lennard-Jones parameters for hydroxyl oxygen from Gromacs forcefield

O_3

Ozone molecule is built from three oxygen atoms in a triangular geometry. The O-O bond length is 0.128nm, the O-O-O angle is 116.6° [32], and atomic charges are slightly increased to implicitly account to polarization effects.

		σ [nm]	ε [kJ/mol]	charge [e]
ljOW[a]	O_{center}	0.3166	0.6502	0.2400
	O_{side}	0.3166	0.6502	-0.1200
ljOA[b]	O_{center}	0.2955	0.8490	0.2400
	O_{side}	0.2955	0.8490	-0.1200
ljOM[c]	O_{center}	0.2626	1.7245	0.2400
	O_{side}	0.2626	1.7245	-0.1200
ljXA[d]	O_{center}	0.2791	1.2100	0.2400
	O_{side}	0.2791	1.2100	-0.1200
ljXW[e]	O_{center}	0.2896	1.0589	0.2400
	O_{side}	0.2896	1.0589	-0.1200
test σ[f]	O_{center}	0.2204	0.6502	0.2400
	O_{side}	0.2204	0.6502	-0.1200
test ε[f]	O_{center}	0.3166	0.9527	0.2400
	O_{side}	0.3166	0.9527	-0.1200

[a] Lennard-Jones parameters for SPC/E water oxygen
[b] Lennard-Jones parameters for hydroxyl oxygen from Gromacs forcefield
[c] Lennard-Jones parameters for carbonyl oxygen from Gromacs forcefield
[d] combination of parameterizations [b] and [c]
[e] combination of parametrizationsparameterizations [a] and [c]
[f] forced parametrization derived from [a]

OH

Hydroxyl radical has a bond lengths of 0.0967nm and it has a dipole moment represented by partial atomic charges[32].

		σ [nm]	ε [kJ/mol]	charge [e]
ljOW[a]	H	0.0000	0.0000	0.4000
	O	0.3166	0.6502	-0.4000
OW-ch50[b]	H	0.0000	0.0000	0.5000
	O	0.3166	0.6502	-0.5000
OW-ch45[b]	H	0.0000	0.0000	0.4500
	O	0.3166	0.6502	-0.4500
ljOA[c]	H	0.0000	0.0000	0.4000
	O	0.2955	0.8490	-0.4000
OA-ch44[d]	H	0.0000	0.0000	0.4400
	O	0.2955	0.8490	-0.4400
OW-ch30[e]	H	0.0000	0.0000	0.3000
	O	0.3166	0.6502	-0.3000
polarOW15[f]	H	0.0000	0.0000	0.4000
	O	0.3166	0.6502	-0.4000
polarOA10[g]	H	0.0000	0.0000	0.4000
	O	0.2955	0.8490	-0.4000

[a] Lennard-Jones parameters for SPC/E water

[b] parametrization derived from [a] by increasing the dipole to partially account for polarization effects

[c] oxygen Lennard-Jones parameters for hydroxyl oxygen from Gromacs forcefield

[d] parametrization derived from [c] by increasing the dipole to partially account for polarization effects

[e] forced parametrization derived from [a]

[f] polarizable model based on model [a] with polarizability of 1.5Å^3 on oxygen

[g] polarizable model based on model [c] with polarizability of 1.0Å^3 on oxygen

HO_2

Hyperoxy radical has a triangular H-O-O geometry with H-O bond length of 0.0975nm and O-O bond length of 0.1324nm. The H-O-O angle is 105.47° [47]. Charges were evaluated using the *ab initio* program package Gaussian03 [48] as a Mullikan charges employing the 6-31g base (charges recalculated with Natural Population Analysis are similar).

		σ [nm]	ε [kJ/mol]	charge [e]
ljOM[a]	H	0.0000	0.0000	0.4454
	O_{center}	0.2626	1.7245	-0.4228
	O_{side}	0.2626	1.7245	-0.0226
ljOA[b]	H	0.0000	0.0000	0.4454
	O_{center}	0.2955	0.8490	-0.4228
	O_{side}	0.2955	0.8490	-0.0226
MSZ[c]	H	0.1390	0.0499	0.4190
	O_{center}	0.2940	0.6277	-0.3580
	O_{side}	0.2940	0.6277	-0.0610

[a] Lennard-Jones parameters for carbonyl oxygen from Gromacs forcefield
[b] Lennard-Jones parameters for hydroxyl oxygen from Gromacs forcefield
[c] parametrization [49]

H_2O_2

The structure of hydrogen peroxide is H-O-O-H, with O-O bond of 0.1468nm and H-O bonds of 0.0968nm long. The H-O-O angle is 98.62° and the dihedral angle is 120°. Charges are calculated by Natural Population Analysis at the MP2/6-31G** level. These values are calculated by Gaussian03 [48].

		σ [nm]	ε [kJ/mol]	charge [e]
ljOW[a]	H	0.0000	0.0000	0.4976
	O	0.3166	0.6502	-0.4976

[a] Lennard-Jones parameters for SPC/E water

XX

The fictitious atom that represent a stationary point does not possess any forcefield parameter except for a mass of 1500 atomic mass units.

Ions

Geometry and charges of H_3O^+ (Eigen hydronium cation) $H_5O_2{}^+$ (Zundel cation) are calculated by Natural Population Analysis with method MP2 in AUG-cc-pVDZ base by program package Gaussian03 [48].

		σ [nm]	ε [kJ/mol]	charge [e]
F^- [a]		0.3132	0.8368	-1.0000
OH^- [b]	H	0.0000	0.0000	0.4238
	O	0.3166	0.6502	-1.4238
$Na_1{}^+$ [c]		0.2350	0.5439	1.0000
$Na_2{}^+$ [d]		0.2730	0.4184	1.0000
H_3O^+ [b]	H	0.0000	0.0000	0.4722
	O	0.3166	0.6502	-0.4166
$H_5O_2{}^+$ [e]	O	0.3166	0.6502	-0.8671
	H_{center}	0.0000	0.0000	0.5636
	H_{iner}	0.0000	0.0000	0.5437
	H_{outer}	0.0000	0.0000	0.5416

[a] parametrization from [50]
[b] parametrization from [51]
[c] parametrization from [52]
[d] parametrization from [53]
[e] Lennard-Jones parameters for SPC/E water

6.3 Appendix C - Simulations details

The constrained method using a spring is implemented in Gromacs[11] version 3.1.5. Because of its non-straightforward behaviour we studied the source code and this is the algorithm: First, the simulation calculates the direction of pulling from the position of center of mass (CM) of reference (RCM) and pulled (PCM) group is established. Then, the position of the PCM is saved as the equilibrium position of the spring (in fact that means that one end of the spring is connected to the beginning of the simulating box and the second end is attached to the PCM). In each step the PCM and the difference between the spring equilibrium position is recalculated. The PCM multiplied by the spring constant (in Gromacs input it is called forceconstant and our default value was $50000\frac{kJ}{mol\,nm^2}$) gives the force acting on the pulled group. This force is written in the output and distributed among atoms in the PCM group proportional to their mass. Finally, the equilibrium position of the spring is changed for the next step by the size of pullrate multiplied by the time step (2fs).

The above analysis leads to the composition of our simulation box. There was a water slab in the middle of the box, which, combined with periodic boundary conditions, yielded an infinite slab with two air/water interfaces. A very heavy fictitious particle with zero interaction placed in the vapour on one side of the slab was called the XX particle. It represented a stationary point that as a reference group defined the direction of pulling. On another side of the slab we placed the solute. During 80 cycles of simulations the solute was pulled through the whole slab towards the XX particle. Based on the symmetry of the slab and slight asymmetry of the PMF, we estimated the error of the PMF to be below 1kJ/mol. This low error was due to the length of the simulation that was 1.5ns for each of the sampling simulations and 20ps for each of the pulling simulations (with the pulled distance of 0.05nm).

This system set up has several advantages which helped us to discover the remaining simulations problems we had to solve. For example, we monitored the force acting on the water slab and compared it with the force affecting the solute. They had exactly the same profile except for the sign as it should be according to the Newton's law of action and reaction. However, there was also a residual additive constant making the forces different. This problem was solved by switching to double precision.

One of the possible problems could be size of the system - the slab has thickness only 2nm. To this end we made a twice bigger slab in the z-direction and the PMF is consistent with the results for the smaller slab yielding the same hydration free energy of N_2 (Fig. 6.1).

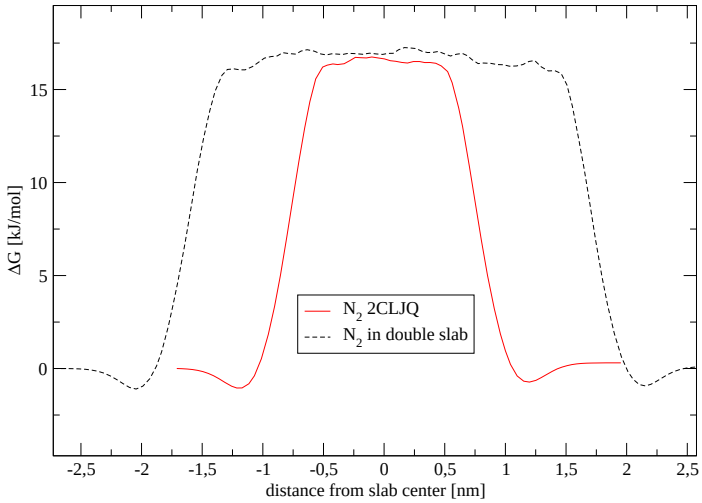

Figure 6.1: The PMF of the nitrogen molecule in two slabs with different size in z-direction.

To demonstrate the computational demands we list the time requirement for typical simulations. One PMF profile needs 80 times 1.5ns long simulations. This takes on a Pentium 4 2.8GHz about three CPU days. Use of PME prolongs the simulation to approximately three CPU weeks. Since the polarizability calculation is even more time consuming, the simulation with polarizable model of water took about three CPU months. All simulations together took about 65.000 hours of computer time.

The standard parameters for thermodynamic integration were: time step 1fs, number of steps 11022000, init_lambda = 0.0, delta_lambda = 0.002, equil = 2000, collect = 20000, ti_equil_nwindows = 9 and ti_equil_ max_slope = 0.00001. Because of the computational intensiveness we did first comparing simulations for different forcefields with cutting off the coulomb interaction (i.e., without PME). The best models were then re-simulated in double precision with PME. The difference using due to PME is shown in the following Table 6.1.

G_{solv}	TI	TI-E	PMF	PMF-E	Experiment
H_2O - SPCE	-28.6	-24.3	-29.3	-28.0	-26.3
H_2O- TIP3P	-25.2	-20.1	-25.7	-25.5	-26.3
N_2- ljX	9.3	8.2	12.8	11.4	10.3 – 10.4
O_2- ljOA	6.0	5.4	9.1	7.7	8.6 – 8.8
O_3 - ljXW	0.2	-0.4	4.4	2.8	2.8 – 3.8
O_3 - ljX	-1.1	-1.5	2.9	1.7	2.8 – 3.8
OH - OA-ch44	-18.1	-14.4	-16.9	-17.6	-16.0 – -21.2
OH - OW-ch50	-18.7	-13.7	-18.3	-18.2	-16.0 – -21.2
OH - polarOA10	-21.9	-18.1	-19.1	-22.1	-16.0 – -21.2
OH - polarOW15	-14.3	-10.4	-13.9	-14.1	-16.0 – -21.2
HO_2 - ljOW	-37.8	-26.6	-32.0	-28.4	-28.7 – -30.7
H_2O_2- ljOW	-40.2	-34.5	-39.4	-41.5	-35.8 – -37.5

Table 6.1: The summary of G_{solv} using different methods and change caused by using PME (-E in caption). Units are in kJ/mol.

6.4 Appendix D - PMFs for of all tested molecular models

Here, we present the simulations in single precision without PME for all the tested molecular models. In the previous parts we chose from these simulations the model which fits best the experimental hydration free energy and with this model we then reran the simulations in double precision and with PME. Note that for ions we were not able for technical reasons (see above) to evaluate the experimental hydration free energy.

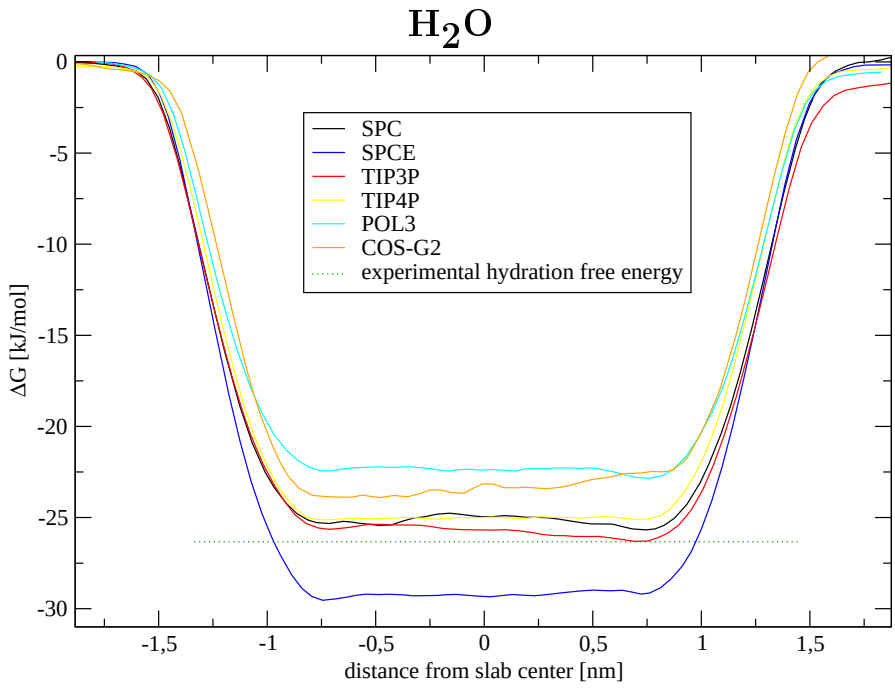

N_2

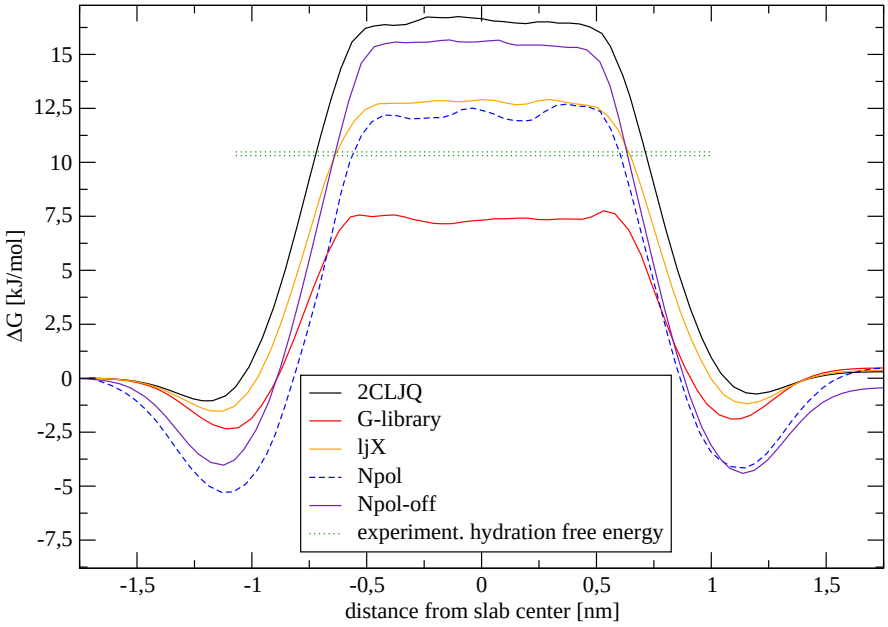
15
12,5
10
7,5
5
2,5
0
-2,5
-5
-7,5
ΔG [kJ/mol]
-1,5
-1
-0,5
0
0,5
1
1,5
distance from slab center [nm]
2CLJQ
G-library
ljX
Npol
Npol-off
experiment. hydration free energy

O_2

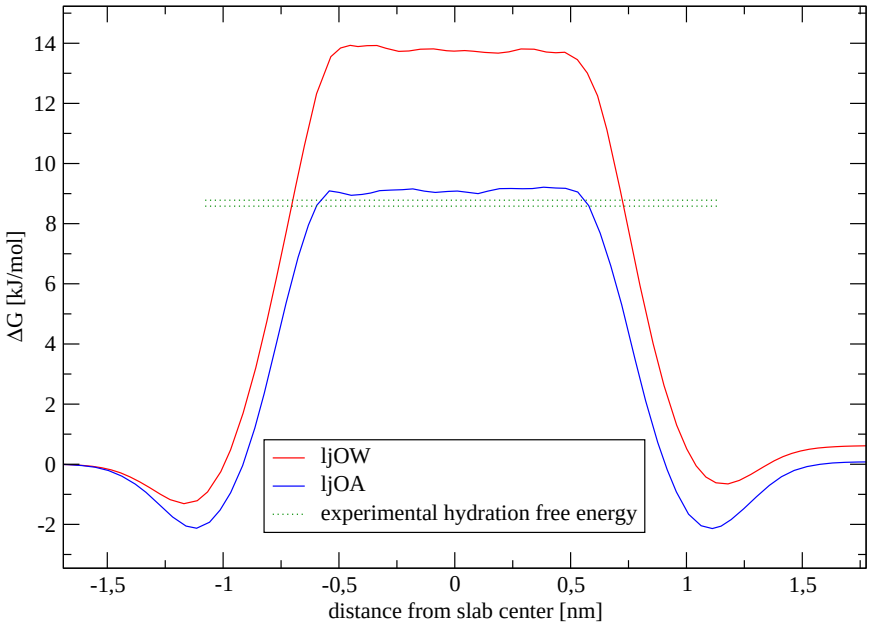
14
12
10
8
6
4
2
0
-2
ΔG [kJ/mol]
-1,5
-1
-0,5
0
0,5
1
1,5
distance from slab center [nm]
ljOW
ljOA
experimental hydration free energy

O_3

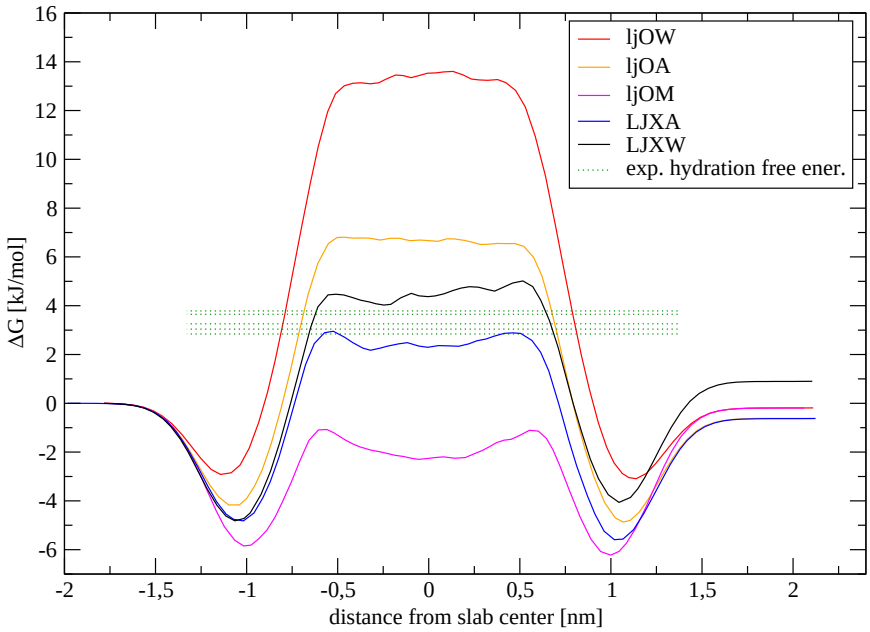
ljOW
ljOA
ljOM
LJXA
LJXW
exp. hydration free ener.
ΔG [kJ/mol]
distance from slab center [nm]

OH

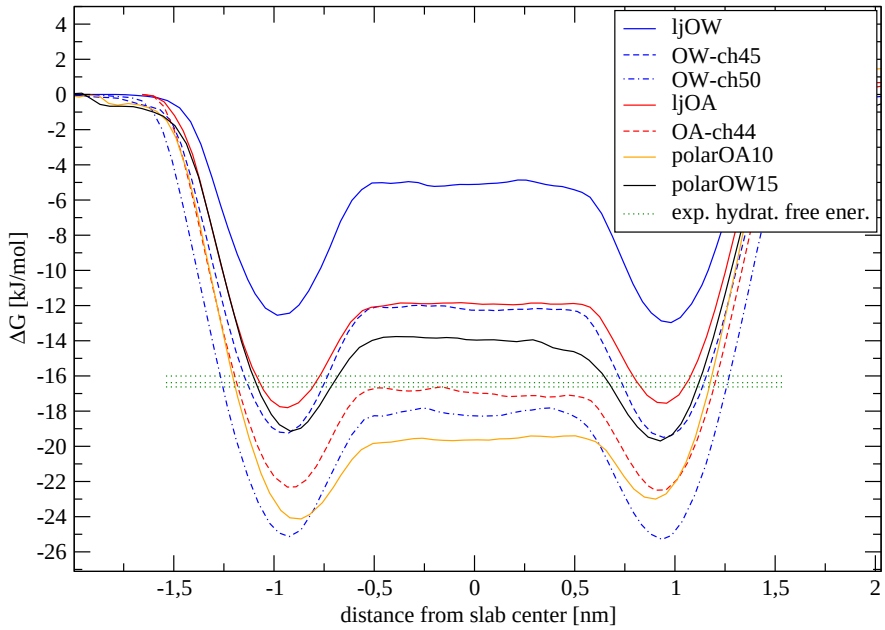
ljOW
OW-ch45
OW-ch50
ljOA
OA-ch44
polarOA10
polarOW15
exp. hydrat. free ener.
ΔG [kJ/mol]
distance from slab center [nm]

HO_2

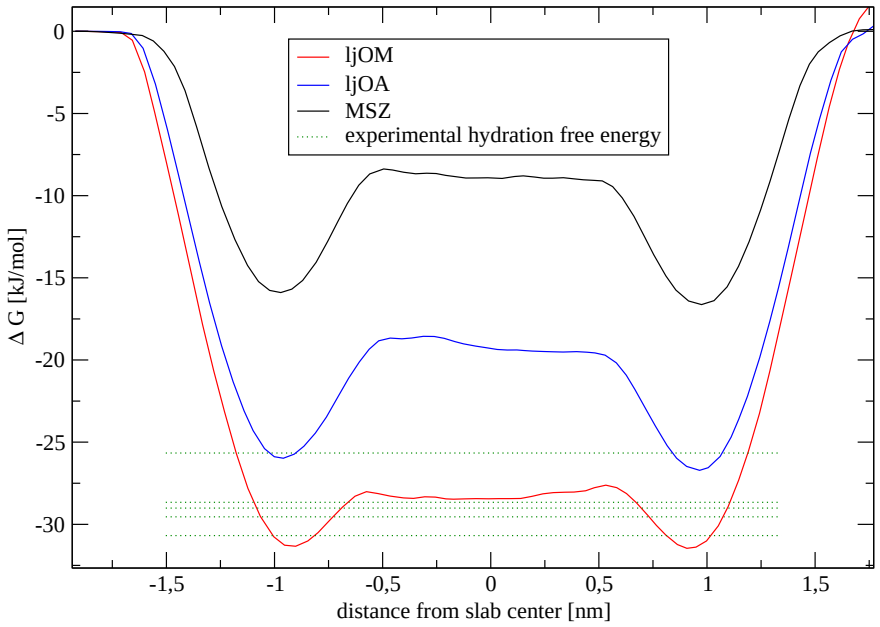
ljOM
ljOA
MSZ
experimental hydration free energy
Δ G [kJ/mol]
distance from slab center [nm]
0
-5
-10
-15
-20
-25
-30
-1,5
-1
-0,5
0
0,5
1
1,5

H_2O_2

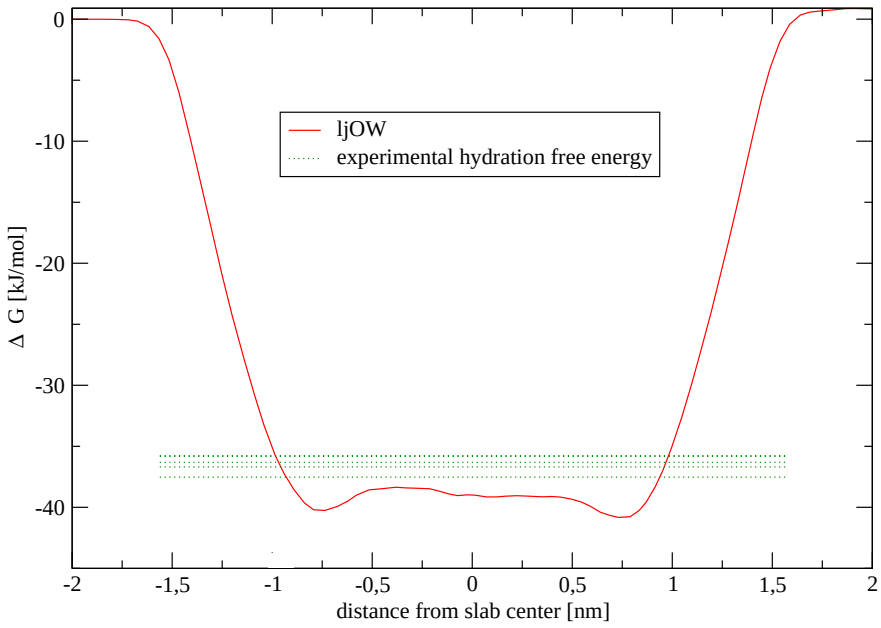
ljOW
experimental hydration free energy
Δ G [kJ/mol]
distance from slab center [nm]
0
-10
-20
-30
-40
-2
-1,5
-1
-0,5
0
0,5
1
1,5
2

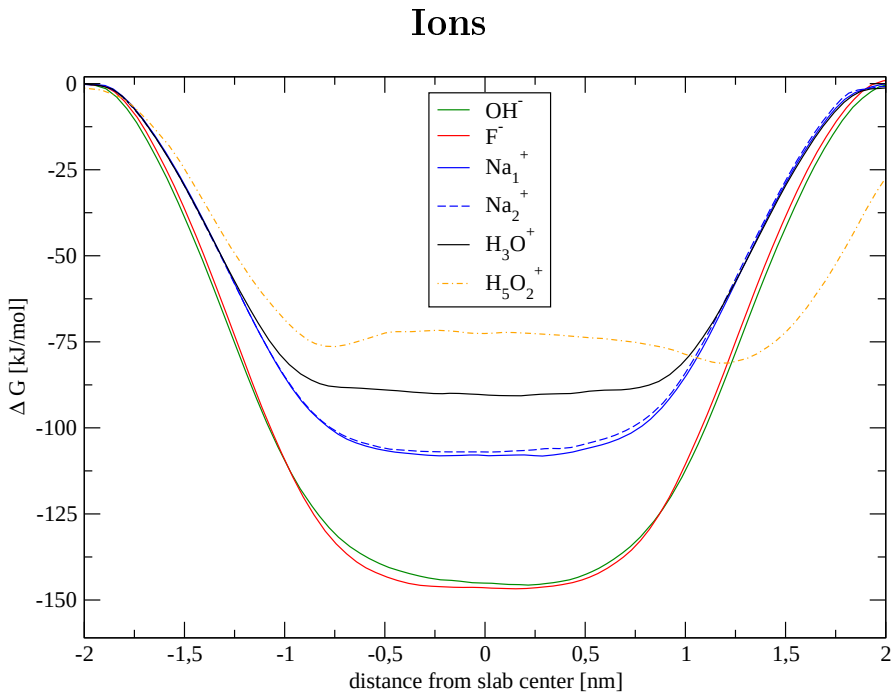
Ions
0
-25
-50
-75
-100
-125
-150
Δ G [kJ/mol]
-2
-1,5
-1
-0,5
0
0,5
1
1,5
2
distance from slab center [nm]
OH-
F-
Na1+
Na2+
H3O+
H5O2+

6.5 Appendix E - Snapshots

Here, we present typical snapshots of the molecules at the water surface.

N_2 O_2 O_3

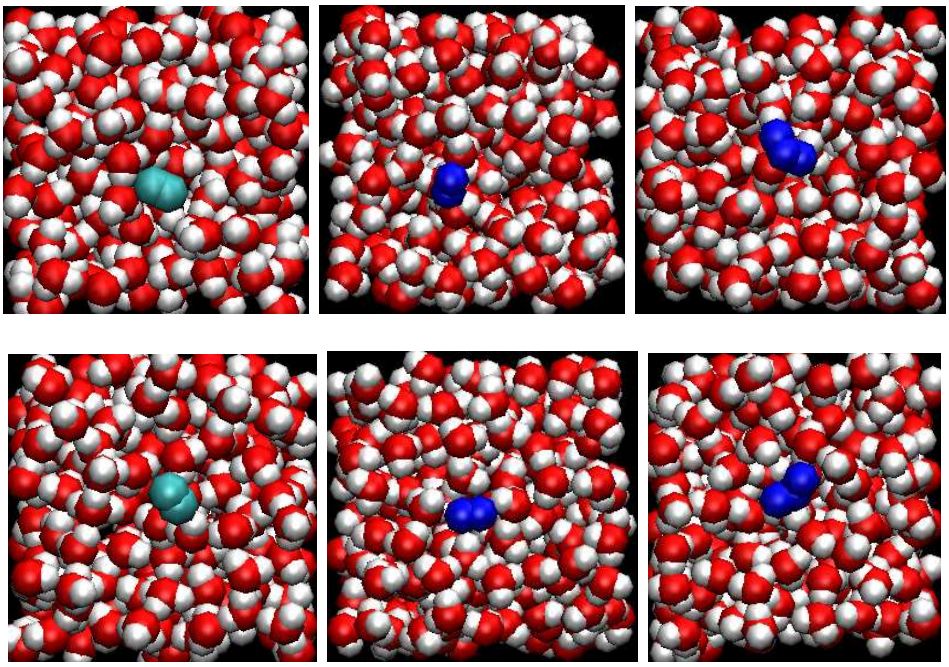

OH HO_2 H_2O_2

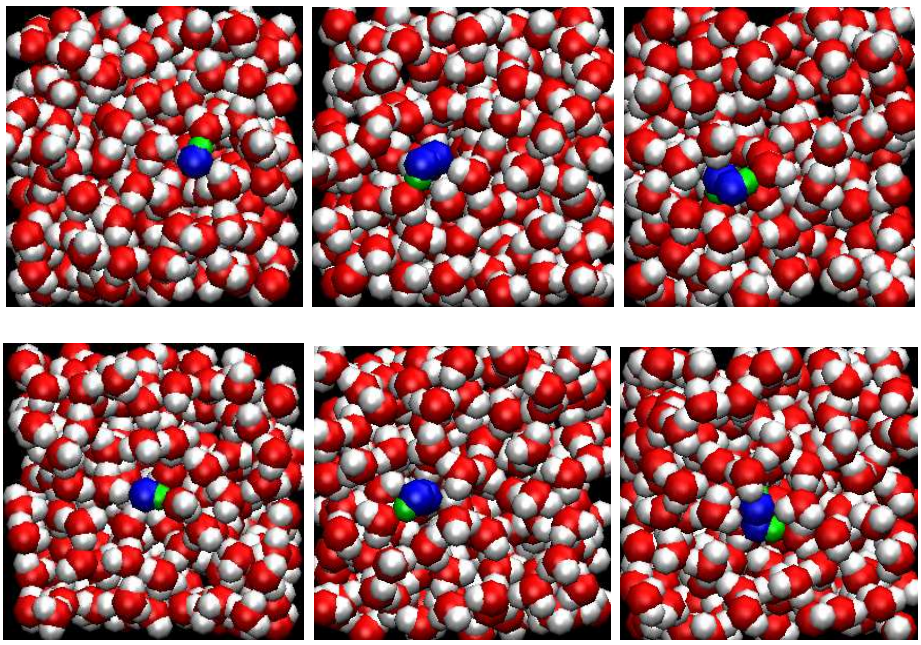

Bibliography

[1] Finlayson-Pitts, B. J., Pitts, J. N.; *Chemistry of Upper and Lower Atmosphere*; Academic Press: San Diego, **2000**

[2] Wayne, P.; *Chemistry of Atmospheres*; Oxford University Press: New York, **2000**

[3] Knipping, E.M., Lanking, M. J., Foster, K. L., Jungwirth, P., Tobias, D. J., Gerber, R. B., Abdub, D., Finlayson-Pitts, B. J.; *Science* **2000**, 288, 301-306

[4] Finlayson-Pitts, B. J.; *Chemical Reviews* **2003**, 103, 4801-4822

[5] Shultz, M. J., Baldelli, S., Schnitzer, C., Simonelli, D.; *Journal of Physical Chemistry B* **2002**, 106, 5313-5324

[6] Raymond, E. A., Richmond, G. L.; *Journal of Physical Chemistry B* **2004**, 108, 5051-5059

[7] Petersen, P. B., Johnson, J. C., Knutsen, K. P., Saykally, R. J.; *Chemical Physics Letters* **2004**, 397, 46-50

[8] Petersen, P. B., Saykally, R. J.; *Chemical Physics Letters* **2004**, 397, 51-55

[9] Defay, R., Prigogine, I.; *Surface tension and adsorption*; Wiley: New York, **1996**

[10] Jungwirth, P., Tobias D. J.; *Journal of Physical Chemistry* **2001**, 105, 10468-10472

[11] Lindhal, E., Hess, B., van der Spoel, D.; *Journal of Molecular Modeling* **2001**, 7, 306-317

[12] Essmann, U., Perera, L., Berkowitz, M. L., Darden, T., Lee, H., Pedersen, L. G.; *Journal of Chemical Physics* **1995**, 103, 8577-8593

[13] Berendsen, H. J. C., Grigera, J. R., Straatsma, T. P.; *Journal of Physical Chemistry* **1987**, 91, 6269-6271

[14] Straatsma, T. P., McCammon, J. A.; *Journal of Chemical Physics* **1991**, 95, 1175-1188

[15] Jorgensen, W. L., Chandrasekhar, J., Madura, J. D., Impey, R. W., Klein, M. L.; *Journal of Chemical Physics* **1983**, 79, 926-935

[16] Zakharov, V. V., Brodskaya, E. N., Laaksonen, A.; *Molecular Physics* **1998**, 95(2), 203-209

[17] Lamourex, G., MacKerell Jr., A. D., B. Roux, B.; *Journal of Chemical Physics* **2003**, 119(10), 5185-5197

[18] Caldwell, J., Dang, L. X., Kollman, P. A., *Journal of the American Chemical Society* **1990**, 112, 9144-914 7

[19] Yu, H., van Gunsteren, W. F.; *Journal of Chemical Physics* **2004**, 121, 9549-9564

[20] Rodriduez-Gomez, D., Darve, E., Pohorille, A.; *Journal of Chemical Physics* **2004**, 108, 3563-3578

[21] Jarzynski, C.; *Physical Review Letters* **1997**, 78, 2690-2693

[22] Jarzynski, C.; *Physical Review E* **1997**, 56, 5018-5035

[23] Crooks, G. E.; *Journal of Statistical Physics* **1998**, 90, 1481-1487

[24] Crooks, G. E.; *Physical Review E* **1999**, 60, 2721-2726

[25] Crooks, G. E.; *Physical Review E* **2000**, 61, 2361-2366

[26] Sander, R.; *Surveys in Geophysics* **1999**, 20,1-31

[27] Bennaim, A., Marcus, Y.; *Journal of Chemical Physics* **1984**, 81, 2016-2027

[28] Sander, R.; "Compilation of Henry's Law Constants for Inorganic and Organic Species of Potential Importance in Environmental Chemistry (Version 3), *www.mpch-mainz.mpg.de/~sander/res/henry.html*" **1999**

[29] Darve, E., Pohorille, A.; *Journal of Chemical Physics* **2001**, 115, 9169-9183

[30] Vrbka, L., Mucha, M., Minofar, B., Jungwirth, P., Brown, E. C., Tobias, D. J.; *Current Oppinion Colloidal Interface Science* **2004**, in press

[31] Taylor, R. S., Ray, D., Garrett, B. C.; *Journal of Physical Chemistry B* **1997**, 101, 5473-5476

[32] Roeselova, M., Jungwirth, P., Tobias, D. J., Gerber, R. B.; *Journal of Physical Chemistry B* **2003**, 107, 12690-12699

[33] Roeselova, M., Vieceli, J. S., Dang, L. X., Tobias, D. J.; *Journal of the American Chemical Society* **2004**, submitted

[34] Dang, L. X., Garrett, B. C.; *Chemical Physics Letters* **2004**, 385, 309-313

[35] Jayne, J.T., Davidovits, P., Worsnop, D. R., Zahniser, M.S. Kolb, C.E.; *Journal of Physical Chemistry* **1990**, 94, 6041-6048

[36] Donaldson, D. J., Guest, J. A., Goh, M. C.; *Journal of Physical Chemistry* **1995**, 99, 9313-9315

[37] Boniface, J., Shi, Q., Li, Y. Q., Cheung, J. L., Rattigan, O. V., Davidovits, P., Worsnop, D. R., Jayne, J. T., Kolb, C. E.; *Journal of Physical Chemistry A* **2000**, 104, 7502-7510

[38] Clegg, S. M., Abbatt, J. P. D.; *Journal of Physical Chemistry A* **2001**, 105, 6630-6636

[39] Tabazadeh, A., Jokelson, R. J., Singh, H. B., Hobbs, P. V., Crawford, J. H., Iraci, L. T.; *Geophysical Research Letters* **2004**, 31, L06114

[40] Mmereki, B. T., Donaldson, D. J.; *Journal of Physical Chemistry A* **2003**, 107, 11038-11042

[41] Jayne, J. T., Gardner, J. A., Davidovits, P., Worsnop, D. R., Zahniser, M. S., Kolb, C. E., *Journal of Geophysical Research-Atmospheres* **1990**, 95, 20559-20563

[42] Vacha, R., Slavicek, P., Mucha, M., Finlayson-Pitts, B. J., Jungwirth, P.; *Journal of Physical Chemistry A* **2004,** 108, 11573-11579

[43] Ewald, P. P.; *Annual Physics* **1921**, 64, 253-287

[44] Dick, B. G., Overhouser, A. W.; *Physics Review* **1958**, 112, 90-103

[45] Vrabec, J., Stoll, J., Hasse, H.; *Journal of Physical Chemistry B* **2001**, 105, 12126-12133

[46] Jordan, P. C.,van Maaren, P. J., Mavri, J., van der Spoel, D., Berendsen, H. J. C.; *Journal of Chemical Physics* **1995**, 103, 2272-2285

[47] Belair, S. D., Kais, S., Francisco, J. S.; *Molecular Physics* **2002**, 100, 247-253

[48] Frisch, M. J.,Trucks, G. W., H. B. Schlegel, G. E. Scuseria, M. A. Robb, J. R. Cheeseman, J. A. Montgomery, Jr., T. Vreven, K. N. Kudin, J. C. Burant, J. M. Millam, S. S. Iyengar, J. Tomasi, V. Barone, B. Mennucci, M. Cossi, G. Scalmani, N. Rega, G. A. Petersson, H. Nakatsuji, M. Hada, M. Ehara, K. Toyota, R. Fukuda, J. Hasegawa, M. Ishida, T. Nakajima, Y. Honda, O. Kitao, H. Nakai, M. Klene, X. Li, J. E. Knox, H. P. Hratchian, J. B. Cross, C. Adamo, J. Jaramillo, R. Gomperts, R. E. Stratmann, O. Yazyev, A. J. Austin, R. Cammi, C. Pomelli, J. W. Ochterski, P. Y. Ayala, K. Morokuma, G. A. Voth, P. Salvador, J. J. Dannenberg, V. G. Zakrzewski, S. Dapprich, A. D. Daniels, M. C. Strain, O. Farkas, D. K. Malick, A. D. Rabuck, K. Raghavachari, J. B. Foresman, J. V. Ortiz, Q. Cui, A. G. Baboul, S. Clifford, J. Cioslowski, B. B. Stefanov, G. Liu, A. Liashenko, P. Piskorz, I. Komaromi, R. L. Martin, D. J. Fox, T. Keith, M. A. Al-Laham, C. Y. Peng, A. Nanayakkara, M. Challacombe, P. M. W. Gill, B. Johnson, W. Chen, M. W. Wong, C. Gonzalez, and J. A. Pople; *Gaussian 03, Revision A.1*; Gaussian, Inc.: Pittsburgh PA, **2003**

[49] Mizan, T. I., Savage, P. E., Ziff, R. M.; *American Institute of Chemical Engeniers Journal* **1997**, 43, 1287-1299

[50] Perera, L., Berkowitz, M. L.; *Journal of Chemical Physics* **1993**, 100, 3085-3093

[51] Brodskya, E., Lyubartsev, A. P., Laaksonen, A.; *Journal of Physical Chemistry B* **2002**, 106, 6479-6487

[52] Perera, L., Berkowitz, M. L.; *Journal of Chemical Physics* **1991**, 95, 1954-1963

[53] Roeselova, M., Jungwirth, P., Tobias, D. J., Gerber, R. B.; *Journal of Physical Chemistry B* **2003**, 107, 12690-12699

Chapter 7

Attached publications